

Figure 1.

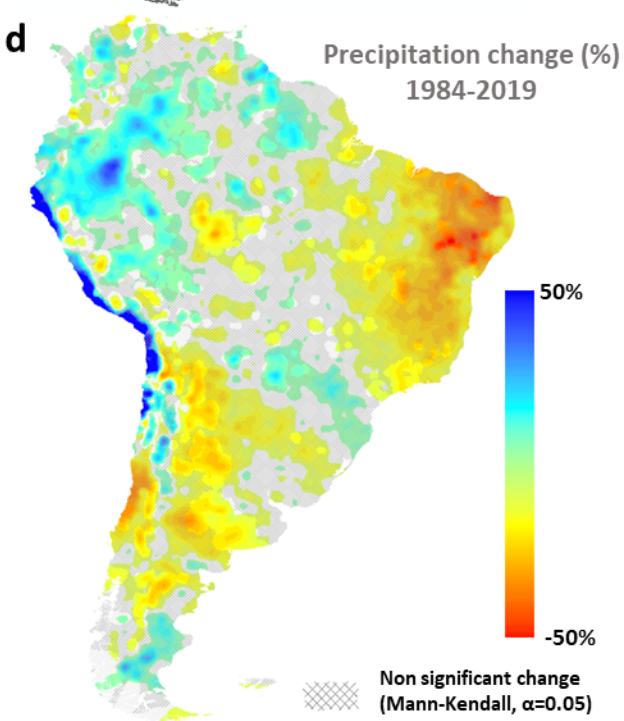
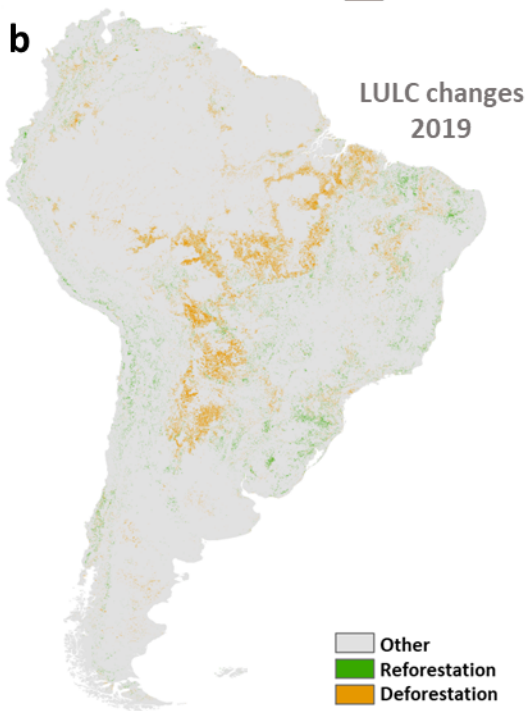
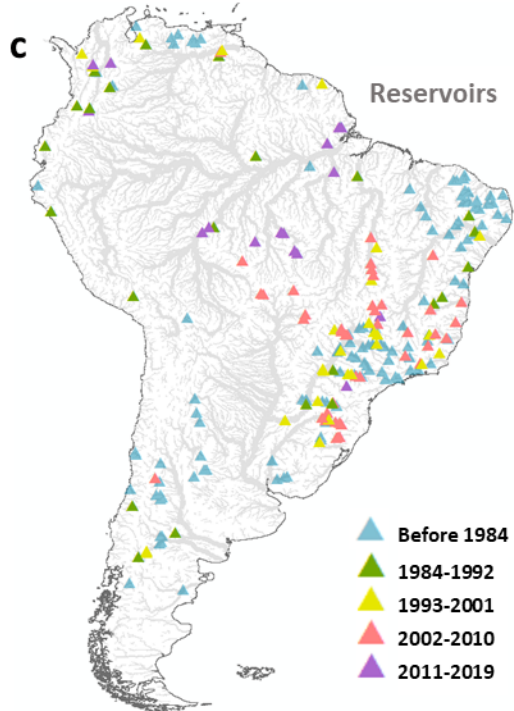
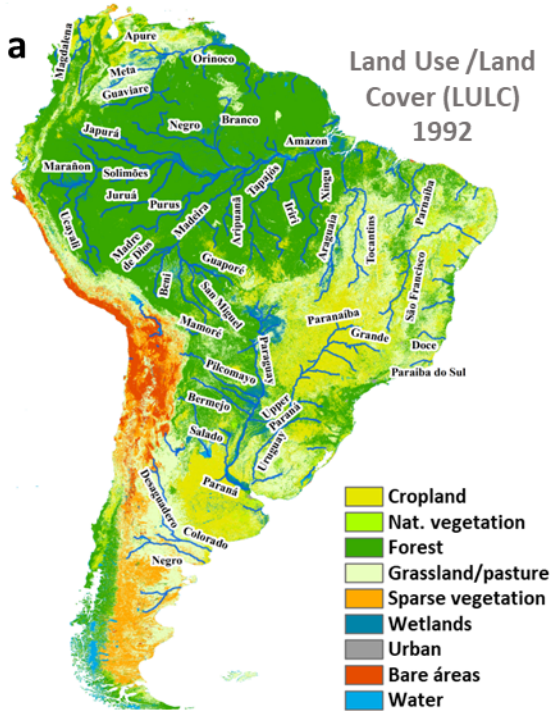
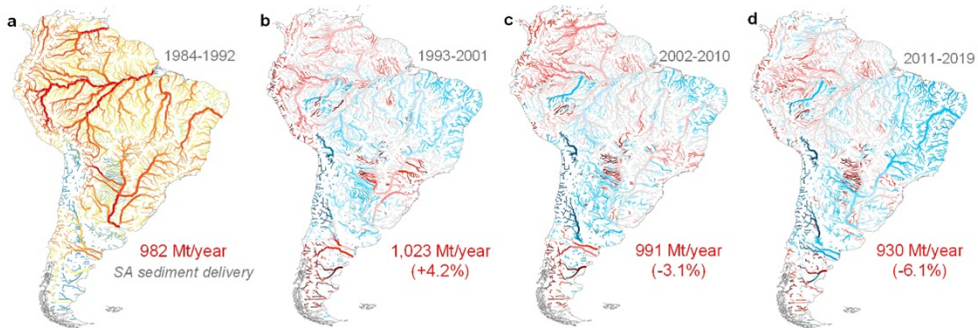
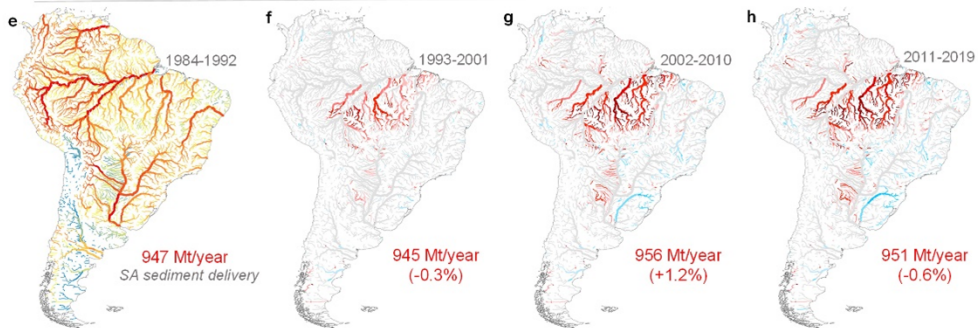


Figure 2.

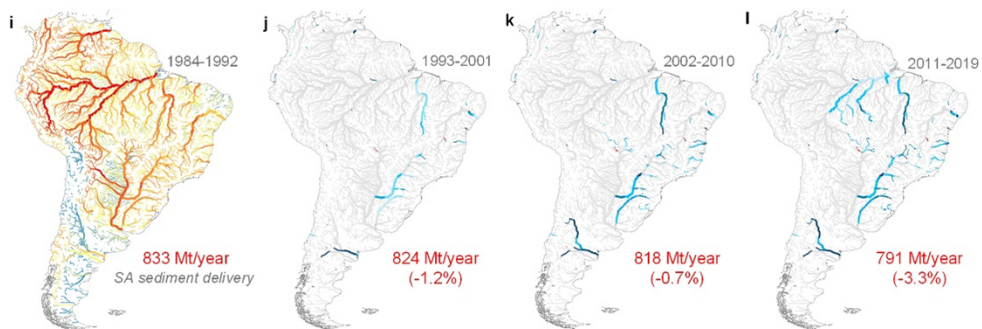
Precipitation effect



LULCC effect



Reservoir effect



SA sediment delivery - combined effects

849 Mt/year

872 Mt/year (+2.7%)

842 Mt/year (-3.5%)

771 Mt/year (-8.4%)

Figure 3.

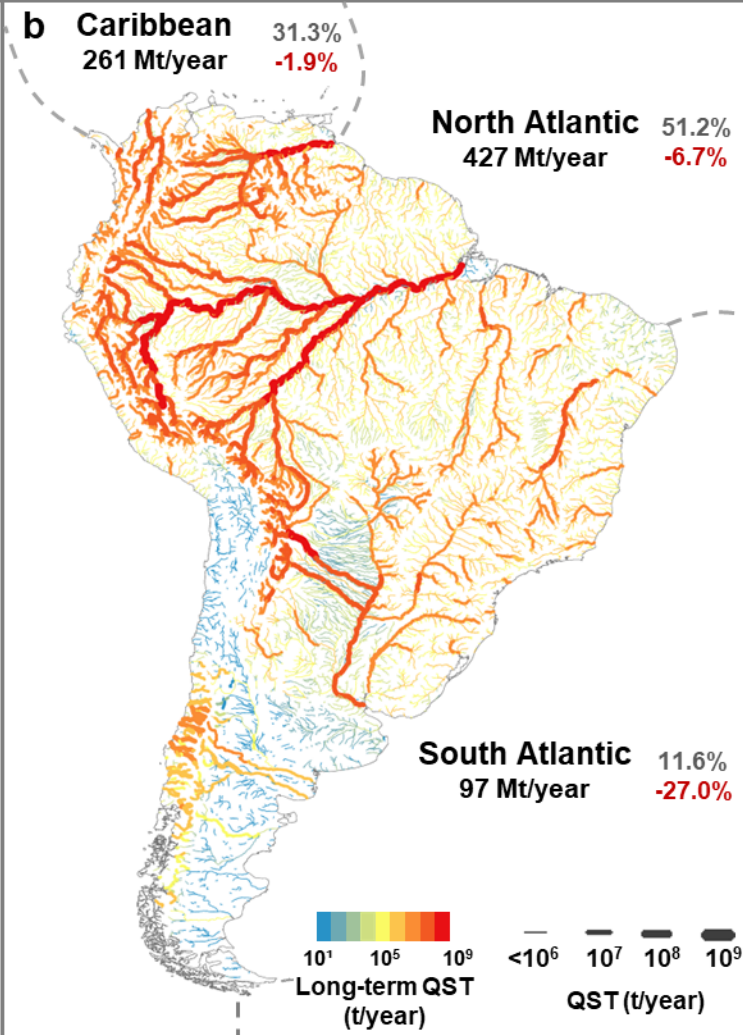
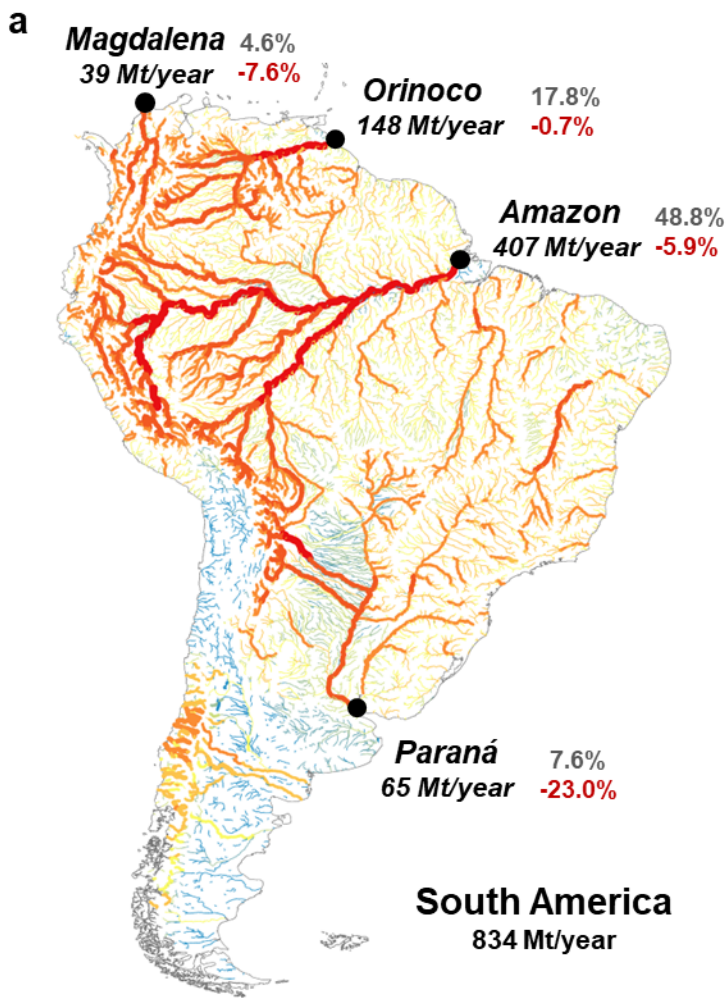
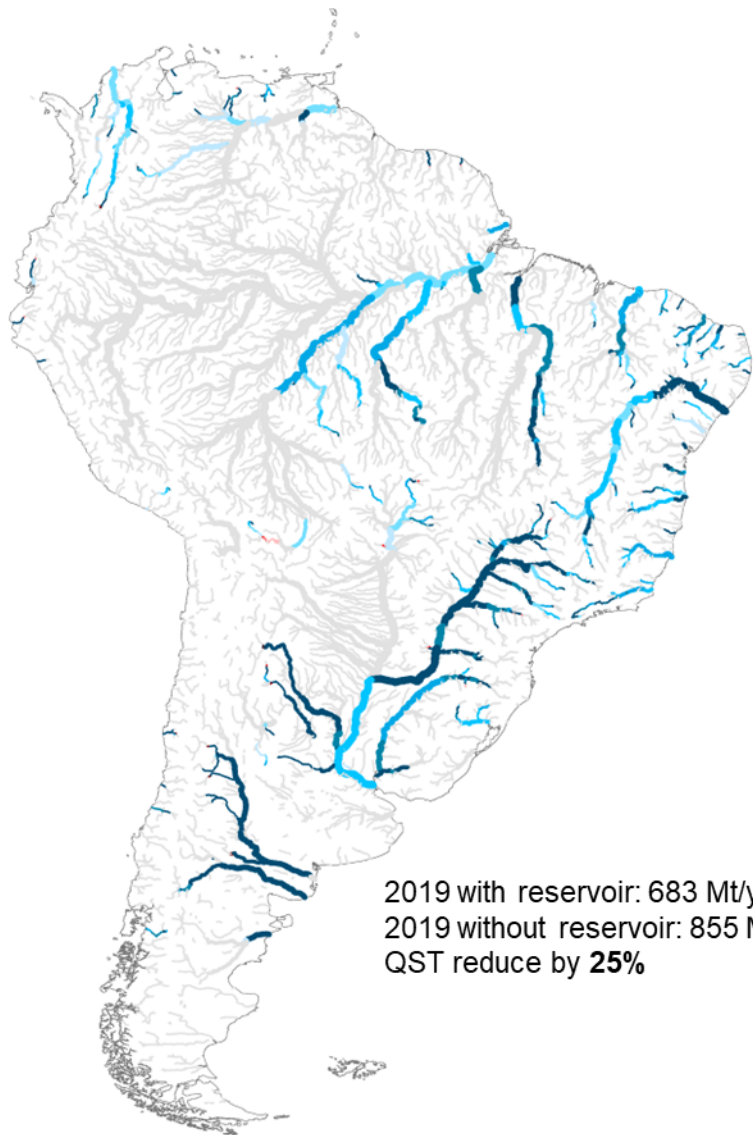


Figure 4.



2019 with reservoir: 683 Mt/year
2019 without reservoir: 855 Mt/year
QST reduce by **25%**

-100 -80 -60 -40 -20 -10 -5 -5 10 20 40 60 80 100
QST change (%)

Figure 5.

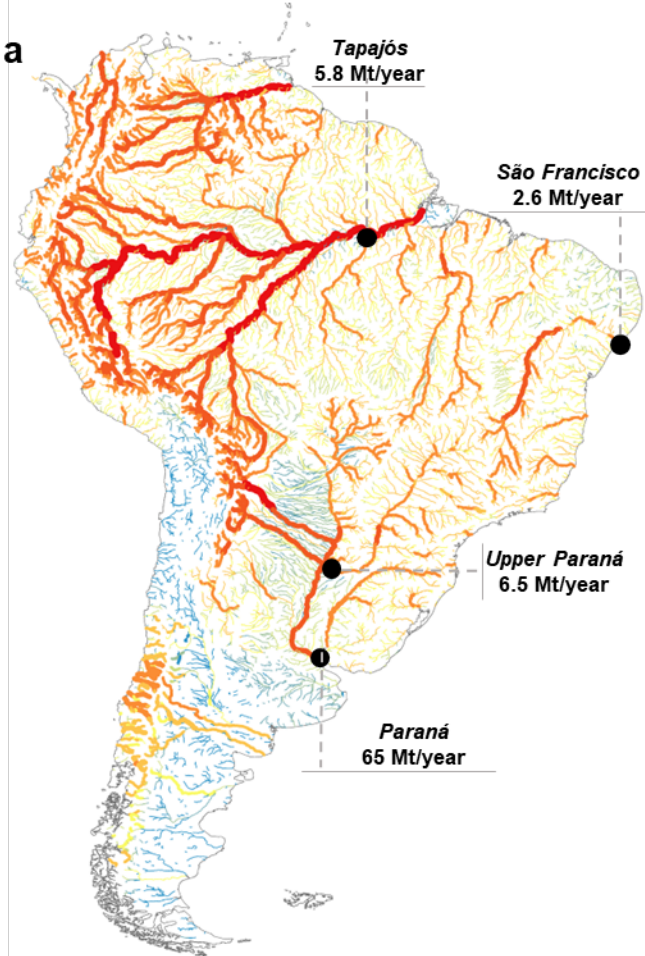
River Sediment Transport in South America

Long-term average (1984-2019)

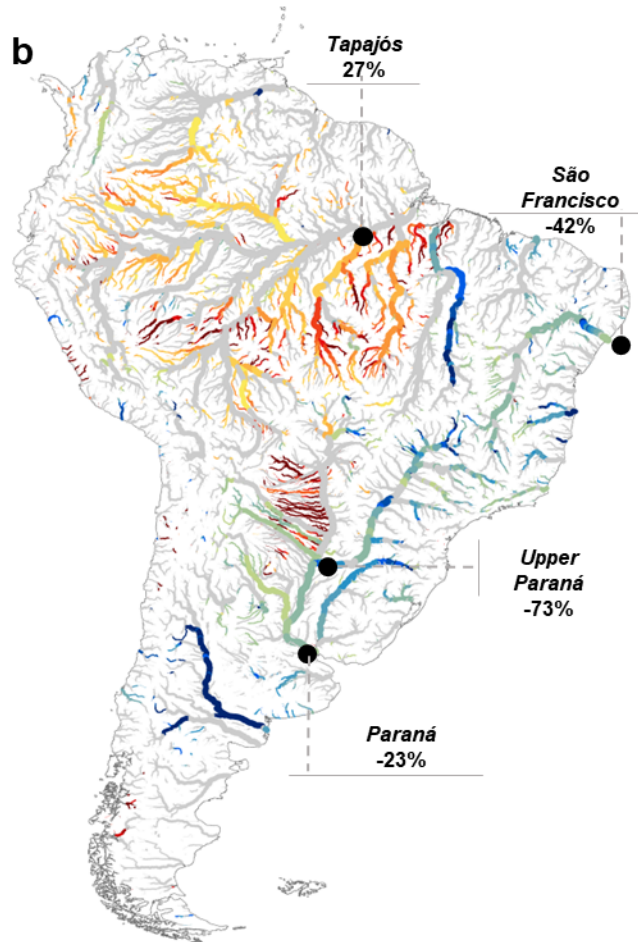
Long-term changes

Main drivers of changes

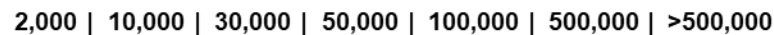
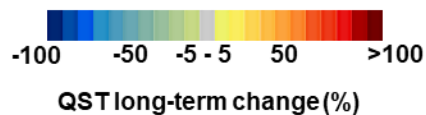
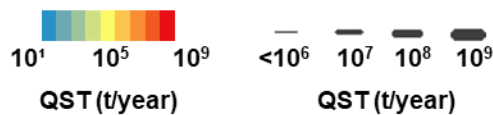
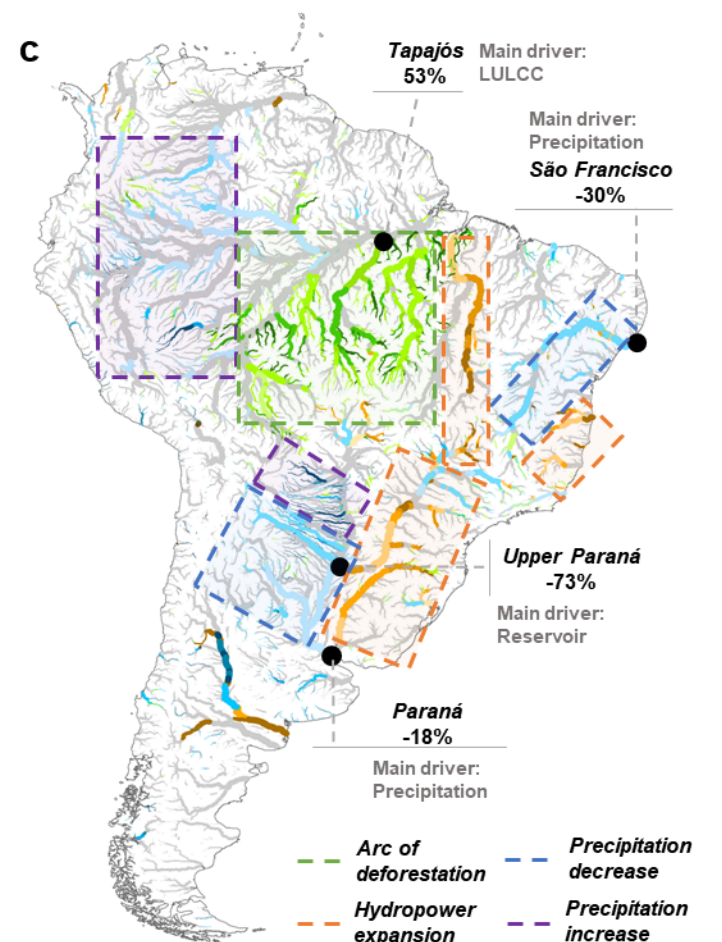
a



b



c



Drainage Area (km²)

1

2 **Human-induced changes in South American sediment fluxes from 1984 to**
3 **2019**

4 H. O. Fagundes^{1,2}, A. S. Fleischmann³, F. M. Fan¹, R. C. D. Paiva¹, D. C. Buarque⁴, V. A. Siqueira¹,
5 W. Collischonn¹, P. Borrelli^{2,5,6}

6 ¹ Institute of Hydraulic Research, Federal University of Rio Grande do Sul, Porto Alegre, Brazil.

7 ² Department of Earth and Environmental Sciences, University of Pavia, Pavia, Italy.

8 ³ Geospatial Analysis of Amazonian Environment and Territories, Mamirauá Institute for
9 Sustainable Development, Tefé, Brazil

10 ⁴ Department of Environmental Engineering, Federal University of Espírito Santo, Vitória, Brazil

11 ⁵ Department of Science, Roma Tre University, 00146 Rome, Italy

12 ⁶ Department of Biological Environment, Kangwon National University, Chuncheon 24341,
13 Republic of Korea

14

15 **Corresponding author:** Hugo de Oliveira Fagundes, h.o.fagundes@hotmail.com

16

17 **Key Points:**

- 18 • Comprehensive analysis of sediment flows changes in SA over the last 36 years
- 19 • 51% of the main SA rivers have undergone significant changes
- 20 • Amazon deforestation and river damming are the main responsible for changes

21

22 **Abstract**

23 Sediment flows dynamics (erosion, transport and deposition) have been disrupted in South

24 America (SA), a continent with the highest erosion and sediment transport rates globally.

25 However, the magnitude and spatial distribution of the main drivers of changes have been

26 poorly identified and explored. Here, we performed simulations using a hydrological-

27 hydrodynamic-sediment model to comprehensively estimate the spatial and temporal sediment

28 changes and trends in SA from 1984 to 2019. We found that 51% of the main SA rivers
29 experienced significant changes in simulated sediment transport (QST) over this period, with
30 36% due to Amazon deforestation and river damming and 15% due to precipitation changes. We
31 also estimated a 10% reduction in the average sediment delivery to the oceans. Deforestation
32 was responsible for QST changes above 80% in some Amazon sites, and hydropower expansion
33 led to a greater reduction of sediment flows (as high as 80-100%) in the Tocantins, Uruguay,
34 Upper Paraná, lower São Francisco, Desaguadero, and Negro rivers. In addition, our results
35 suggest that reservoirs built in the Amazon region in the last decade are also affecting sediment
36 transport. Our modeling outputs provide unprecedented information about the status of
37 sediment dynamics in SA, and a means to develop evidence-based strategies and transboundary
38 policies related to continental-wide sediment dynamics and the conservation and restoration of
39 ecosystems.

40 **Keywords:** Sediment transport, large-scale modeling, reservoir, land use.

41

42 1 Introduction

43 Sediment flows (erosion, transport and deposition) play an essential role providing social,
44 economic, and environmental services. The surface flow, rich in organic and inorganic
45 compounds, supports healthy agriculture and natural fertilization (Montanarella et al., 2016),
46 provides nutrients for aquatic ecosystems (Best, 2019), and helps maintain the structural
47 stability of rivers, shorelines, mangroves, and wetlands (Costanza et al., 1997; Ezcurra et al.,
48 2019; Nagel et al., 2022). However, sediment flows (sand, silt and clay) have been considerably
49 disrupted by accelerating human-induced erosion, sediment trapping in dams, and long-term

50 changes in precipitation patterns (Ezcurra et al., 2019; Grill et al., 2019; Latrubesse et al., 2017;
51 Quinton et al., 2010).

52 Over the last three decades, 60% of South America (SA) territory experienced land use and land
53 cover changes (LULCC), with extensive areas converted into pastures, cropland, and tree
54 plantations, mainly in the Chaco and Amazon ecosystems (Zalles et al., 2021). Over the same
55 period, more than 100 large reservoirs were constructed, with a storage capacity of more than
56 400 billion cubic meters, affecting aquatic species throughout SA. The continent has more than
57 6,800 reservoirs (Mulligan et al., 2020), of which more than 340 are large reservoirs (Lehner et
58 al., 2011). In addition, 1,300 hydroelectric generation reservoirs are under construction or
59 planned in the continent (Zarfl et al., 2015), with 288 only in the Amazon region (Latrubesse et
60 al., 2017). These numbers constantly change due to the new developments and environmental
61 licensing procedures. In addition, several flood and drought events have been recorded in
62 recent years (Cai et al., 2020), with increasing precipitation trends in the Amazon region and
63 decreasing precipitation in Central Argentina and the Brazilian Northeast.

64 These ongoing changes can induce detrimental effects on SA ecosystems (e.g., Central Amazon
65 floodplains and Pantanal), one of the world's richest locations in terms of above-ground, soil,
66 and aquatic biodiversity (Albert et al., 2021; Barbarossa et al., 2020; Kemppinen et al., 2020).
67 For example, unsustainable agricultural expansion requires more fertilizers (Borrelli et al., 2017),
68 which can be responsible for both the water bodies eutrophication and damage to human
69 health (Dissanayake and Chandrajith, 2009). In addition, the reservoirs storage capacity can be
70 considerably reduced by aggradation, threatening the water supply (Wisser et al., 2010). In
71 contrast, lower sediment delivery to the oceans can induce the erosion of coastal terrestrial
72 ecosystems (Ezcurra et al., 2019). Also, floodplains and mangroves are very productive areas

73 (Costanza et al., 1997) that can be eroded by reducing sediment to the rivers, making them a
74 source of carbon to the atmosphere instead of a sink (Ezcurra et al., 2019). Moreover, a
75 disturbance in sediment flows can also affect the meander migration, generating social and
76 economic damage to riverine communities (Nagel et al., 2022).

77 Therefore, it is essential to understand the magnitude of changes in sediment fluxes, their
78 associated key drivers, and their role in mitigating ecosystem degradation effects. New insights
79 are needed to narrow the knowledge gap for river sediment dynamics, especially for large
80 geographical domains encompassing transboundary regions like SA river systems. However, the
81 lack of observed data represents a major barrier to develop analyses for large scales
82 (continental or global) that require long time series for many sites (Best, 2019). For these scales,
83 no studies with in situ data have been found in the literature. The most notable work published
84 recently used remote sensing data to show changes in global sediment fluxes (Dethier et al.,
85 2022). However, this work did not show the climatic influence on sediment supply and focused
86 on assessing changes at the mouths of major rivers. This approach does not provide a broad
87 understanding of the sediment processes that occur in the basin. For example, it is known that
88 the concentration of sediments at the mouth of the Amazon River tends to be higher than in
89 upstream regions due to local processes such as resuspension (Fassoni-Andrade and Paiva,
90 2019). An isolated analysis of this process occurring at the mouth can lead to a misinterpretation
91 of the processes occurring throughout the basin.

92 In this way, large-scale assessments of sediment fluxes are usually performed using global
93 sediment transport models to characterize their spatial or temporal dynamics. These models
94 were developed to estimate the impact of human activities on sediment delivery to the oceans
95 (Syvitski et al., 2005), characterize rivers in terms of transported sediment loads (Cohen et al.,

96 2013; Pelletier, 2012), and assess regional trends and variabilities (Cohen et al., 2014). However,
97 they do not typically attempt to understand the relative contributions of precipitation, dams,
98 and LULCC on sediment fluxes. From the literature, we noted that most studies focused on
99 describing changes in sediment fluxes by considering one or two of these drivers (Almagro et al.,
100 2017; Diodato et al., 2020; Forsberg et al., 2017; Huang et al., 2020; Latrubesse et al., 2017;
101 Syvitski et al., 2009; Vörösmarty et al., 2003; Wei et al., 2019), and few have provided detailed
102 analyses on these changes (Huang et al., 2020; Wei et al., 2019). Some studies have performed
103 integrated analyses with all the aforementioned drivers, but the information was presented for
104 specific locations or with a broad perspective (Li et al., 2020; Macklin and Lewin, 2019).

105 This study provides the first comprehensive analysis of the spatiotemporal changes in sediment
106 fluxes in SA over the last 36 years (1984 to 2019), accounting for changes in precipitation, dams,
107 and land use and land cover (LULC). To pursue this goal, we simulated multiple scenarios with
108 the continental-scale sediment model MGB-SED AS (acronym in Portuguese for 'Modelo de
109 Grandes Bacias', Fagundes et al., 2021) using daily precipitation, eight LULC maps, and 234 large
110 dams. In addition, relationships between these changes and impacts on ecosystems are
111 presented. These simulations enabled us to isolate each driver's contribution and also to assess
112 their combined effects on sediment flows.

113

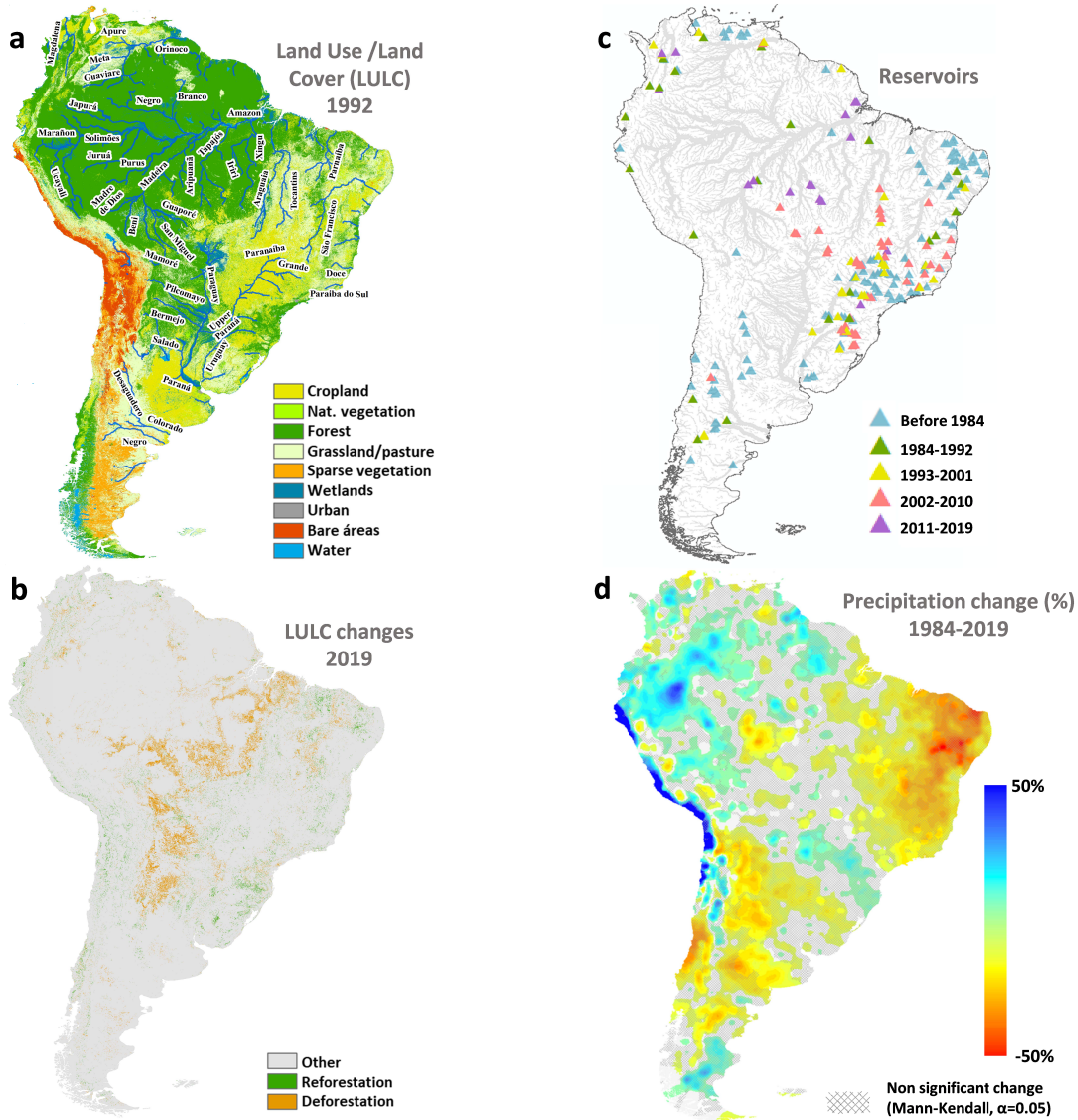
114 2 Study area

115 South America (SA, Figure 1-A) is one of the continents with the highest erosion and sediment
116 transport rates globally (Borrelli et al., 2017; Doetterl et al., 2012; Latrubesse et al., 2005), has a
117 large biodiversity (Kemppinen et al., 2020), is one of the few regions having free-flowing rivers

118 (Grill et al., 2019), and contributes significantly to global food production (Sartori et al., 2019).
119 Most of SA is located in tropical regions that have little interannual variability between sunrise
120 and sunset and receive high solar incidence. The Intertropical Convergence Zone (ITCZ) directly
121 influences the establishment of dry and rainy seasons; El Niño events; and the South Atlantic
122 Convergence Zone (SACZ), which causes heavy precipitations in the summer. Annual
123 precipitation variability is strong, with desert regions in Chile (0.05 to 10 mm/year, Bozkurt et
124 al., n.d.) and very humid regions in Colombia (~10,000 mm/year, Latrubesse et al., 2005). The
125 Amazon, Orinoco, Paraná and Magdalena rivers are the main sediment transporters, meaning
126 44%, 14%, 11% and 3%, respectively, of total South America sediment discharges values to the
127 ocean (Fagundes et al., 2021). In addition, floodplains in SA has an important role in retaining
128 12% of total suspended sediment carried by the rivers (Fagundes et al., 2021).

129 However, the rapid expansion of agriculture on the continent (Figure 1-B) in recent decades
130 (Song et al., 2018; Zalles et al., 2021) is accompanied by increasing erosion rates, directly
131 affecting food production and the economy (Borrelli et al., 2017; Sartori et al., 2019). In
132 addition, many existing reservoirs (Figure 1-C) have been reducing the sediment load in rivers
133 and oceans (Syvitski et al., 2005), causing negative impacts in these regions (Syvitski et al.,
134 2009). Nevertheless, the concern is even greater with SA planned reservoirs (see Figure S1 -
135 Supporting Information S1), especially in the Amazon region, as they may dramatically affect
136 river connectivity (Grill et al., 2019), sediment exchange between rivers and floodplains
137 (Latrubesse et al., 2017), biodiversity (Albert et al., 2021; Barbarossa et al., 2020), fish migration
138 (Forsberg et al., 2017), and deltas (Dunn et al., 2019). SA has also been showing changes in
139 annual precipitation (Figure 1-D), with increasing trends in intense rainfalls in some regions (e.g.

142 Amazon, Diodato et al., 2020), while others have experienced severe droughts in recent years
 143 (e.g. Northeast Brazil, Marengo et al., 2022).



143
 150 **Figure 1. Overview of South America changes.** a, main changes in land use/ land cover
 151 between 1992 and b, 2019, using LULC data from European Space Agency ([http://www.esa-](http://www.esa-landcover-cci.org/)
 152 [landcover-cci.org/](http://www.esa-landcover-cci.org/)). c, 234 large dams (storage capacity > 10^6m^3) from Yigzaw dataset (see
 153 methods section), *Brazilian Water National Agency* and *Brazilian National Electric System*
 154 *Operator*. d, trends of precipitation changes from 1984 to 2019 using daily precipitation from
 155 the Multi-Source Weighted Ensemble Precipitation – MSWEP v1.1 dataset until 2014, and from
 156 2015 onward using the NASA Global Precipitation Measurement Mission – GPM dataset.

150 3 Methods

151 **3.1 Modeling South American hydrology and sediments: the MGB-SED AS model**

152 The MGB-SED model results from the coupling of a sediment module (Buarque, 2015) with the
153 MGB hydrological model (Collischonn et al., 2007; R. C. D. Paiva et al., 2011; Pontes et al., 2017).

154 This model has shown ability to simulate sediment erosion, transport and deposition at large
155 scales (Fagundes et al., 2019, 2021, 2020; Föeger et al., 2022), and the hydrological module has
156 been applied in many tropical watersheds to address different questions (Fleischmann et al.,
157 2019a, 2018; R. C. D. Paiva et al., 2011; Pontes et al., 2017; Siqueira et al., 2018).

158 The MGB-SED AS model (Fagundes et al., 2021) was developed to investigate the spatial and
159 temporal dynamics of suspended sediment flows in South America. This model resulted from
160 the coupling between the sediment module and the hydrologic-hydrodynamic model MGB-SA,
161 presented by Siqueira et al. (2018). According to Fagundes et al. (2021), this configuration was
162 mainly chosen due: (i) MGB-SA is the first fully coupled hydrologic-hydrodynamic model,
163 developed for regional scales, applied for SA's continental domain; and (ii) the model has a high
164 temporal resolution (daily outputs) and was validated in most of SA using in situ and other
165 sources of hydrological data, showing that hydrological variables were well represented
166 (graphical and statistical analysis). Both MGB-SA (Siqueira et al., 2018) and MGB-SED AS
167 (Fagundes et al., 2021) showed better performance to global models in simulate hydrological
168 and sediment variables. The MGB-SED AS model (Fagundes et al., 2021) simulates suspended
169 sediment flows for the medium to large South American (SA) rivers (river reaches with drainage
170 areas larger than 1,000 km²). The model has a sediment module(Buarque, 2015) coupled to the
171 MGB-SA hydrologic-hydrodynamic model (Siqueira et al., 2018). The main model's forcing
172 variable is the daily precipitation and it was calibrated and validated in most continental areas

173 using in situ data for both hydrological and sediment variables. The model is described in the
174 following sections.

175 **3.1.1 Hydrological-hydrodynamic module**

176 The MGB-SA is a continental-scale hydrologic-hydrodynamic model developed for the South
177 American domain (Siqueira et al., 2018). It uses simplified mathematical relations to describe
178 runoff generation processes and physically based equations to compute evapotranspiration and
179 channel routing processes. The main hydrological processes simulated by the model are (i)
180 canopy interception; (ii) soil infiltration; (iii) evapotranspiration; (iv) routing of surface,
181 subsurface, and groundwater runoff (hillslope routing); and (v) hydrodynamic propagation in
182 river networks.

183 The model is discretized using a semi-distributed approach, where basins are divided into unit-
184 catchments according to the underlying topography and a pre-defined river length, and further
185 into Hydrological Response Units (HRUs) based on combinations of soil type and land cover.
186 Vertical water balance and evapotranspiration (calculated with Penman-Monteith equation) are
187 computed at the HRU level, and river routing is computed at the unit-catchment scale.

188 (Pontes et al., 2017)(Collischonn et al., 2007)(Kouwen et al., 1993)MGB-SA uses the local inertial
189 equation (Bates et al., 2010) to route streamflow along the drainage network and to compute
190 stored volume, flooded area, discharge, and river water levels. The water surface elevation is
191 assumed homogeneous along a given unit-catchment. Recent works have assessed the impact
192 of spatial discretization on MGB simulated variables and have shown that the effect on river
193 discharges tends to be small compared with those on water level and flood extent (Fan et al.,
194 2021a; Fleischmann et al., 2019b). Floodplains are represented as storage areas in which water
195 can be lost through evaporation. Infiltration of floodplain water into the unsaturated soils is also

196 computed. When compared with the full 1D Saint-Venant equations, the local inertial method is
 197 relatively simple as it has an explicit solution, and has been successfully applied to represent
 198 low-slope rivers and floodplain effects in flood inundation/river routing models with scales
 199 ranging from regional (Fleischmann et al., 2018; Getirana et al., 2017) to global (Yamazaki et al.,
 200 2013). On the other hand, it requires a smaller time step (typically 3-4 minutes) to avoid
 201 numerical instability, and has limitations to simulate river regimes with relatively high flow
 202 velocity as the advective inertia term – which is neglected in the local inertial model – may
 203 become important (Bates et al., 2010; Pontes et al., 2017, Fleischmann et al., 2018)

204 **3.1.2 Sediment module**

205 The sediment module is divided into basin, river, and floodplain modules. The basin module
 206 computes rill and interrill erosion of hillsides using the Modified Universal Soil Loss Equation
 207 (MUSLE – Equation 1)(Williams, 1975).

$$Sed = \alpha \cdot (Q_{sur} * q_{peak} * A)^{\beta} \cdot K \cdot C \cdot P \cdot LS_{2D} \quad (1)$$

208 where Sed [t/day] is the sediment yield, Q_{sur} [mm/day] is the specific runoff volume, q_{peak}
 209 [m³/s] is the peak runoff rate, A [ha] is the unit-catchment area, K [0.013 · t · m² · h/m³ · t · cm]
 210 is the soil erodibility factor, C [dimensionless] is the cover and management practices factor,
 211 P [dimensionless] is the conservation practices factor, LS_{2D} [dimensionless] is a bidimensional
 212 topographic factor, and α and β are the equation fit coefficients, with values originally
 213 estimated at 11.8 and 0.56 (Williams, 1975), respectively. We used the same parameter values
 214 set for the first application of the MGB-SED AS model (Fagundes et al., 2021).

215 The sediment volume estimated by MUSLE is divided into three particle classes (sand, silt, and
 216 clay) and is discharged into the river through three linear reservoirs, that store these

217 sedimentsIn the river drainage network, each of three sediment loads is routed from upstream
 218 to downstream. Fine loads (silt and clay) are routed using the 1D advection transport equation
 219 without the diffusion term, and the sediments are transported in suspension without deposition
 220 in the channel. Sands, considered bedload, are routed using the Exner sediment continuity
 221 equation and the Meyer-Peter and Müller transport capacity equation to quantify the channel's
 222 transport, erosion, or deposition (Buarque, 2015).

223 The characteristic diameters adopted for silt and clay particles were 0.016 mm and 0.001 mm,
 224 respectively. These assumed values have led to satisfactory results in a previous study (Fagundes
 225 et al., 2021). We began our simulations using a characteristic sand diameter value of 0.1 mm.
 226 However, because bedload has strongly heterogeneous characteristic diameters, especially
 227 when rivers with high and low slopes are compared, we developed an empirical equation to
 228 estimate the characteristic sand diameter. After an exhaustive search for South American
 229 bedload data in several journals and repositories (in Portuguese, Spanish, and English), we
 230 selected the D50 diameter from 14 river reaches (Carvalho, 2009; Fantin-Cruz et al., 2020; Filho,
 231 2016; Latosinski et al., 2017; J. B. D. de Paiva et al., 2011; Paiva, 1988, 2007; Rizzardi, 2013;
 232 Strasser, 2008; Wiegand, 2009). We performed a unique regression ($R^2=0.21$) using D50
 233 diameter against the slope ($Sl, m/km$) (estimated from a Digital Elevation Model - DEM),
 234 yielding Equation 2:

$$D_{sand} = 0.4476Sl^{0.0776} \quad (2)$$

235 where D_{sand} (m) is the characteristic diameter of sand for a specific river reach.

236 In the floodplain module, suspended sediment exchanges between rivers and floodplains are
 237 computed assuming that floodplains have a zero longitudinal velocity and complete mixing.

238 These assumptions imply that concentrations of silt and clay are uniform in the vertical profile.
 239 Sediment deposition is computed using the fall velocity equation (Equation 3)(Wu and Wang,
 240 2006). Sediments that are not deposited flow back to the main channel.

$$\omega_j = \frac{Mv}{Nd} \left[\sqrt{\frac{1}{4} + \left(\frac{4N}{3M^2} D_{*,j}^3 \right)^{\frac{1}{np}}} - \frac{1}{2} \right]^{np} \quad (3)$$

241

242 where

$$M = 53.5e^{-0.65Sp} \quad (4)$$

$$N = 5.65e^{-2.5Sp} \quad (5)$$

$$np = 0.7 + 0.9Sp \quad (6)$$

$$D_{*,j} = d \left[\frac{\left(\frac{\rho_s}{\rho} - 1 \right) g}{v^2} \right]^{\frac{1}{3}} \quad (7)$$

243

244 and where v is water kinematic viscosity (10^{-6} m²/s); Sp is the Corey shape factor, taken as 0.7
 245 (WU, 2008); d [m] is the representative nominal diameter of the particle class; $D_{*,j}$ is the non-
 246 dimensional diameter for the j particle size; ρ_s/ρ is the sediment-specific gravity; and g is the
 247 gravity acceleration (9.8 m/s²).

248 **3.1.3 Reservoir module**

249 Within the MGB-SED AS model framework, the representation of reservoirs involves the
 250 regulation of water inflows at a given dam location and sediment trapping along the reservoir
 251 lake. These two aspects are detailed in the following two sections.

252 *3.1.3.1 Water regulation by dams*

253 The regulation effect of a given dam is simulated using an offline routine, i.e., the
 254 hydrodynamics of a given unit-catchment associated with a dam are replaced by a level-pool
 255 routine (lumped reservoir). Thus, the dam inflow is estimated as the inflow to that unit-
 256 catchment, using a uniform flow as the boundary condition for upstream unit-catchments with
 257 an average water slope estimated from the DEM. The dam level-storage relationship is obtained
 258 from national and global reservoir databases. Direct lake evaporation was also included and
 259 computed using the Penman equation (Shuttleworth, 1993).

260 The dam outflow is simulated with a simple operation scheme (Hanasaki et al., 2006; Shin et al.,
 261 2019). The suitability of this scheme for estimating large-scale reservoir regulation was recently
 262 shown (Fleischmann et al., 2021) for a test case of more than 30 reservoirs in the Paraná River
 263 Basin in Brazil. They concluded that although the proposed approach (Shin et al., 2019) is generic
 264 and simple, it provides reasonable estimates and is useful in evaluating regional hydrologic
 265 regime scale alterations.

266 The adopted scheme is a daily inflow-and-demand-based rule suitable for hydropower dams,
 267 which do not withdraw water from the system. This approach is reasonable for South America,
 268 where most dams are used for hydropower generation. Equation 8 defines the dam outflow:

$$Q(i, t) = R_i K_{i,y} I_m + (1 - R_i) I_t \quad (8)$$

269 where $Q(i, t)$ is the i th dam outflow at daily time step t , R_i is a regulation capacity constant that
 270 can be calibrated with observations or estimated with Equation 9 (Shin et al., 2019), and is
 271 assumed to be equal zero for run-of-the-river dams ($R_i < 0.1$). I_m and I_t are the annual average
 272 and daily dam inflows, respectively, and $K_{i,y}$ is the storage fraction at the beginning of the
 273 hydrological year (Equation 10). The hydrological year of each dam is defined as the month
 274 where the naturalized (pristine) flow falls below the average (i.e., the beginning of drawdown
 275 season) (Hanasaki et al., 2006).

$$R_i = \min(1, \alpha c_i) \quad (9)$$

$$K_{i,y} = S_{first,y} / \alpha C_i \quad (10)$$

277 The term c_i is the ratio of the maximum dam storage C_i to the annual average dam inflow
 278 ($c_i = C_i / I_m$), $S_{first,y}$ is the storage at the beginning of the hydrological year y , $\alpha_{res} C_i$ is the
 279 target storage, and α_{res} is a constant set to 0.85 (Hanasaki et al., 2006). I_m was calculated based
 280 on a prior long-term MGB simulation (1984–2019), including dynamic land cover and climate,
 281 but not reservoirs. This approximation is reasonable because reservoir regulation has a minor
 282 impact on the long-term average discharge (mainly through evaporation).

283 After estimating $Q(i, t)$, the reservoir storage is updated using equation 11, which represents a
 284 lumped (concentrated) reservoir:

$$V_{act}(i, t) = V_{act}(i, t - 1) + (I_t - Q(i, t)) * 86400 \quad (11)$$

285 where $V_{act}(i, t)$ is the i th dam volume at daily time step t .

286 On the first simulation day for a given reservoir (i.e., the first day of either the MGB simulation
 287 or the dam inauguration year), it was assumed to be full. The dams were inserted into the model

288 in their respective inauguration years to account for the interannual changes in dam storage
 289 across the continent.

290 As described next,, a set of equations (12-15) were adopted to ensure the stability of the
 291 numerical scheme and to prevent unphysical behavior (e.g., to avoid negative storage).

292 For the run-of-the-river reservoirs:

- 293 • If the reservoir storage is under 90% after computing $Q(i, t)$ and $V_{act}(i, t)$, we compute a
 294 new discharge (Equation 12) and volume (Equation 11).

$$Q^1(i, t) = Q(i, t) - \frac{V_{max} - V_{act}(i, t - 1)}{86400} \frac{V_{act}(i, t - 1)}{V_{max}} \quad (12)$$

295 where $Q^1(i, t)$ is the updated discharge for daily time step t .

- 296 • If this scheme results in a negative volume, we return to the original values estimated
 297 using Equation 11 and compute a new outflow discharge using Equation 13.

$$Q^1(i, t) = 0.01 \frac{V_{act}(i, t - 1)}{86400} \quad (13)$$

- 298 • If Equation 12 instead results in a negative discharge, we re-compute the updated
 299 discharge as:

$$Q^1(i, t) = Q(i, t) - 0.01 \frac{V_{act}(i, t - 1)}{86400} \quad (14)$$

300 For the reservoirs that are not run-of-the-river reservoirs:

- 301 • If the reservoir storage is above 98% (almost overtopping) after computing $Q(i, t)$ and
 302 updating the reservoir storage (V_{act}):

$$Q^1(i, t) = Q(i, t) + \frac{V_{act} - 0.98 V_{max}}{(1 - 0.98)V_{max}} (\max(0.0, I_t - Q(i, t))) \quad (15)$$

- 303 • If the reservoir storage is under 20% after computing $Q(i, t)$ and $V_{act}(i, t)$, we follow the
 304 process described above for run-of-the-river reservoirs when they are less than 90% full.

305 3.1.3.2 Sediment deposition in reservoir

306 To represent the deposition of fine sediments (silt and clay) in reservoirs, we used Equation
 307 16(Julien, 2010),

$$C(i, t, j) = Co(i, t, j)e^{\frac{-X_i \omega_j}{h_i u_i}} \quad (16)$$

308 where $C(i, t, j)$ is the i th dam downstream sediment concentration at daily time step t for the j
 309 particle size (silt or clay); $Co(i, t, j)$ is the i th dam upstream sediment concentration at daily
 310 time step t for the j particle size; X_i is the i th dam longitudinal length; ω_j is the settling velocity
 311 (Equation 3) for the j th particle size; h_i is the i th dam average depth (Equation 17); u_i is the i th
 312 dam longitudinal velocity (Equation 18).

$$h_i = \frac{V_{act}}{Ares_i} \quad (17)$$

313 where $Ares_i$ is the i th dam surface area.

$$u_i = \frac{I_t}{h_i \left(\frac{Ares_i}{X_i} \right)} \quad (18)$$

314 For coarse sediments (sands), we assumed that the total load arriving in the reservoir is
 315 deposited.

316 **3.2 MGB-SED AS input data and parameterization**

317 The MGB–SA simulations used the 15 arcsec HydroSHEDS flow direction map (Lehner et al.,
318 2008) and a 1,000km² minimum drainage area threshold. The unit-catchment discretization
319 used a fixed river length of 15km. Floodplain topography was estimated at the sub- unit-
320 catchment level using the Height Above Nearest Drainage (HAND) computed from the Bare-
321 Earth SRTM v.1 DEM (O’Loughlin et al., 2016). The river hydraulic geometry (bankful width and
322 depth) was specified using a global dataset (Andreadis et al., 2013) with additional information
323 from regional studies (Beighley and Gummadi, 2011; Paiva et al., 2013; Paiva et al., 2011;
324 Pontes, 2016). Manning's roughness coefficient was set to 0.03 for the entire continent, as is
325 typical in large-scale hydrodynamic modeling (Siqueira et al., 2018).

326 The simulation from 1984 to 2019 was performed using daily precipitation from the Multi-
327 Source Weighted Ensemble Precipitation – MSWEP v1.1 dataset (Beck et al., 2017) until 2014
328 and using the NASA Global Precipitation Measurement Mission – GPM dataset (Skofronick-
329 Jackson et al., 2017) from 2015 onward. For the GPM data, a correction of the precipitation bias
330 was performed so that the values were more compatible with the MSWEP data. This correction
331 was performed using the quantile-quantile method, parameterized by the gamma function.
332 Long-term averages (climate normals) for surface air temperature, atmospheric pressure,
333 incoming shortwave solar radiation, relative humidity, and wind speed were obtained from the
334 Climate Research Unit (CRU) Global Climate v.2 data (New et al., 2002)and were used to
335 compute evapotranspiration.

336 While a previous application using the MGB-SED AS (Fagundes et al., 2021) used the South
337 America HRU’s map (Fan et al., 2015) to simulate the influence of land use and land cover (LULC)
338 changes, we used eight LULC maps from European Space Agency (<http://www.esa-landcover->

339 cci.org/) and built the HRU's maps for the following years (simulated period): 1992 (1984-1992),
340 1995 (1993-1995), 1998 (1996-1998), 2001 (1999-2001), 2005 (2002-2005), 2010 (2006-2010),
341 2015 (2011-2015) and 2019 (2016-2019). We used a short interval in the early years because
342 according to literature (Zalles et al., 2021) LULC changes in this period were higher than those
343 observed in the recent years. The maps have spatial resolution of 300m. We used the same base
344 of the South America HRU's map (Fan et al., 2015) to represent soil type (shallow and deep).

345 The input data to compute the MUSLE equation in the sediment module is the same as used in
346 the previous application of the MGB-SED AS. The K factor is computed based on the
347 percentages of silt, clay, sand, and organic carbon comprising the soil from the Food and
348 Agriculture Organization (FAO) of the United Nations (FAO/UNESCO, 1974); LS_{2D} is based on the
349 Bare-Earth SRTM v.1 DEM (O'Loughlin et al., 2016); P is assumed to be 1; and C is computed as
350 in previous studies (Benavidez et al., 2018; Buarque, 2015; Fagundes et al., 2021). For each HRU
351 map, the C values changed according to soil cover.

352 The major difference between the MGB-SED AS version used here and the previous version
353 (Fagundes et al., 2021) is the inclusion of sediment trapping by reservoirs at the continental
354 level. Here, we used 234 large dams (storage capacity $> 10^6\text{m}^3$) from the Yigzaw dataset (Yigzaw
355 et al., 2018), *Agência Nacional de Águas do Brasil* (ANA) and *Operador Nacional do Sistema*
356 *Elétrico do Brasil* (ONS). ANA and ONS are Brazilian state agencies. The reservoirs were selected
357 using the following three criteria: (i) they are currently operational; (ii) there are available level-
358 area-volume relationships; (iii) they are not located in headwater unit-catchments (i.e., a
359 drainage area of $\sim 1.000\text{ km}^2$). Using area and volume information, we fitted a fourth-degree
360 polynomial for each reservoir, which was used to compute the daily surface area from the daily

361 stored volume. When the longitudinal dam lengths were unavailable, they were estimated using
 362 visual analysis and geographic information system tools from satellite images.

363 **3.3 Validation of the reservoir and sediment modules**

364 Reservoirs were validated comparing water discharge from 376 in-situ stations against
 365 simulated data with and without reservoirs. Using observed and simulated data we computed
 366 the Skill Score (SC, Equation 19, Figure S2 - Supporting Information S1) for the Nash-Sutcliffe
 367 coefficient (*NSE*, Nash and Sutcliffe, 1970).

$$SC = \frac{NSE_{reservoir} - NSE}{1 - NSE} \quad (19)$$

368 The validation of river discharge for 12 gauges located on major regulated river reaches across
 369 the continent is presented in Figure S3 - Supporting Information S1. The validation of the
 370 simulated reservoirs' volumes and dam outflows using the MGB-SED AS model is shown in
 371 Figure S4 - Supporting Information S1. The results demonstrate reasonable model performance,
 372 especially in simulating dam volumes dynamics, which is an important variable affecting
 373 sediment trapping in the MGB-SED AS model (Equations 16, 17 and 18).

374 After including the reservoirs and obtaining satisfactory results from the model when
 375 incorporating LULC changes, we carried out a few manual adjustments to α and β MUSLE
 376 parameters values through trial and error. The model performance for sediment flows was
 377 evaluated in three different stages: (i) we computed percent BIAS (%) of simulated suspended
 378 sediment discharge (QSS, silt+clay) relative to observed QSS, considering the period of 1992–
 379 2009 and the same 595 sediment stations used in the previous MGB-SED AS simulation
 380 (Fagundes et al., 2021). Observed data were obtained from *Agência Nacional de Águas do Brasil*,
 381 *Base de Dados Hidrológica Integrada da Argentina* (BDHI) and *Instituto de Hidrologia*,

382 *Meteorologia e Estudos Ambientais da Colômbia* (IDEAM) used in the previous MGB-SED AS
383 simulation (Fagundes et al., 2021) (Figure S5 - Supporting Information S1); (ii) we compared the
384 annual and daily simulated and observed sediment bedload (Figure S6 - Supporting Information
385 S1). Bedload data were collected from local and regional studies (Alarcón et al., 2003;
386 CNEN/CDTN - Centro de Desenvolvimento da Tecnologia Nuclear and IFNMG/Campus Januária -
387 Instituto Federal do Norte de Minas Gerais, 2020; Gamaro et al., 2014, 2011; Latrubesse et al.,
388 2009; Martins et al., 2009; Martins and Stevaux, 2005; SZUPIANY et al., 2005) using other
389 approaches (e.g., acoustic techniques to monitor fluvial ripples). It should be mentioned that
390 both daily and annual bedload data are extremely scarce for large South American rivers.

391 In the Figure S7 - Supporting Information S1, we present an example of the reservoir effect in
392 simulated suspended sediment concentration downstream large dams, comparing two
393 simulations considering the presence and absence of reservoirs against observed data from
394 ANA.

395 **3.4 Long-term analysis of sediment changes**

396 We performed three main analyses to understand how sediment fluxes have changed since
397 1984. Our simulations assumed that precipitation changes daily, reservoirs begin operating from
398 their first operating year (if this occurred before 1984, its operation begins at the start of the
399 simulation), and LULCC. We started the simulations in 1979 and used five years to warm up the
400 model. Three main scenarios were then simulated to isolate the effect of each driver
401 (precipitation, LULC, and reservoirs), and a final simulation was run to understand the
402 synergistic effects of these drivers on sediment flows:

- 403 • *Precipitation changes scenario* – LULC map of 1992, reservoir module disabled, and daily
404 precipitation from 1984 to 2019.

- 405 • *Reservoir changes scenario* – LULC map of 1992, reservoir module enabled, and 2012
 406 daily precipitation. A daily precipitation series of 36 years was created by repeating the
 407 2012 data. We tested several years, and 2012 was chosen because it represents the
 408 median precipitation during the whole simulation period for the entire South American
 409 continent.
- 410 • *LULC changes scenario* – all LULC maps, reservoir module disabled, and 2012 daily
 411 precipitation.
- 412 • *Combined effects scenario* - all LULC maps, reservoir module enabled, and daily
 413 precipitation from 1984 to 2019.

414 The first analysis focused on temporal changes. The entire simulated period (36 years) was
 415 divided into four nine-year periods (1984–1992, 1993–2001, 2002–2010, 2011–2019). We then
 416 computed the annual total sediment discharge (QST) for each scenario and averaged it over
 417 each period. We designated 1984–1992 as the baseline period and computed the relative
 418 change for the others (Equation 20).

$$\text{Changes (\%)} = 100x \frac{QST_{tf} - QST_{1984-1992}}{QST_{1984-1992}} \quad (20)$$

419 where tf is the future period (1993–2001, 2002–2010 or 2011–2019).

420 The second analysis focused on the global changes using only the combined effects scenario to
 421 identify rivers with significant changes. Here we used two statistical criteria to define significant
 422 changes: 1) the QST long-term change in a given river was above 5%; 2) the change was
 423 statistically significant to the 5% level using the Mann-Kendall test (M-K test, Kendall and
 424 Gibbons, 1975). The QST long-term change was computed using linear regression (time vs. QST)
 425 for the entire simulated period by comparing the first and last points of the fitted line. We used

426 this approach instead of Equation 20 because we observed that the QST series exhibited great
427 variability due to interannual precipitation variability, which could be misinterpreted if only 9-
428 years averages were considered. For example, the last period (2011–2019) was quite dry over
429 much of eastern South America, and this phenomena could be erroneously interpreted as a
430 trend. In addition to the criteria presented, rivers were considered significantly affected when
431 they presented significant QST changes in more than 40% of the main river length.

432 The third and final analysis was carried out to identify the main driver responsible for change for
433 each river with a significant change. We observed that changes in the QST series were more
434 abrupt when only reservoirs or LULC changes were considered, especially because they are
435 timely progressive. However, precipitation changes were more variable, with alternations of dry
436 and wet periods. Therefore, to compute long-term changes (%) appropriately for each driver, we
437 used Equation 20 for the Reservoir changes and LULC changes scenarios and the linear
438 adjustment for the Precipitation changes scenario.

439 Although we computed changes in sediment fluxes for many rivers in South America, we
440 focused our analyses on the major rivers. The major rivers were classified as those with drainage
441 areas greater than 100,000 km² and simulated QST without reservoirs greater than 1,000,000
442 t/year. The latter criterion was adopted because it considers more natural river conditions.
443 More than one driver could be dominant for specific river reaches in some large rivers. In such
444 cases, the dominant driver was selected based on two criteria: i) if the river was partially
445 affected by both precipitation and LULC, the driver with more range in the river's downstream
446 portion was selected; ii) the reservoir driver was selected when its effect was observed in a
447 stretch with a drainage area greater than 50% of the basin's drainage area.

448

449 4 Results and discussions

450 **4.1 Model validation and caveats**

451 Our modeling outputs agree with previous regional studies. For instance, our analyses suggested
452 that sediment flows are increasing in the Upper Tapajós due to deforestation and the
453 consequent increase of erosion (Oestreicher et al., 2017), and increasing in other several regions
454 of Amazon due to precipitation increase (Diodato et al., 2020). At the same time, we estimated a
455 reduction in sediment flows in the Bermejo River due to the precipitation decrease in its upper
456 basin (González and Murgida, 2012), and most recently, in the Lower Madeira and Lower
457 Tapajós rivers due to reservoir building (Grill et al., 2019; Latrubesse et al., 2017).

458 Our model was satisfactorily validated in simulating reservoir dynamics. By using 376 gauge
459 stations located downstream of dams, streamflow estimates were improved by 40% when
460 compared to simulations without reservoirs (Figure S2 - Supporting Information S1). We also
461 compared our daily simulated QSS against data from 595 in situ sediment stations (Figure S5 and
462 Figure S7 - Supporting Information S1). In 60% of the stations, the relative error *BIAS* was
463 between -50% and 100%. We noted an improvement in QSS estimates after including the
464 reservoirs, especially for the São Francisco (Figure S7 - Supporting Information S1), Paraná, and
465 Tocantins rivers, compared to a previous study using the same model (Fagundes et al., 2021).
466 We also compared simulated daily and annual bedload (sand) values against regional estimates,
467 with *BIAS* values of 582% and 233%, respectively (Figure S6 - Supporting Information S1). These
468 last differences are reasonable for analyses using annual data such as those conducted in this
469 study.

470 Sediment studies require considerable data, often acquired via traditional approaches using in
471 situ measurements. However, even in this era of big data and big science, there remains a lack

472 of hydrological and sediment data on the world's large rivers (Best, 2019). This picture is even
473 worse when the subject is bedload data. For example, after extensive research in literature,
474 databases, and private institutions, we achieved bedload data only for 11 sites (Figure S6 -
475 Supporting Information S1) in the whole South America domain. This lack of data points to the
476 great challenge in making measurements (that provide reliable results) of bed load in large
477 rivers and the insufficient investment in this field of science.

478 Therefore, sediment modeling becomes an alternative to support spatial and temporal analysis
479 but still requires good input data and validation processes (Fagundes et al., 2021). In this study,
480 our main limitation was the lack of observed data to calibrate some model components.
481 Furthermore, although Bolivia and Venezuela are regions with high sediment yield, we could not
482 obtain data from these countries. Other limitations include the insufficient representation of
483 lateral erosion, that can be important for meandering rivers (Nagel et al., 2022), as well as gully
484 erosion and landslides that are relevant sediment processes especially for Andean rivers, like
485 Bermejo and Pilcomayo, and can induce underestimates in these regions (Borrelli et al., 2017).
486 In addition, due to our continental domain of analysis, some simplifications were necessary and
487 can be a source of uncertainties. These include equations that represent processes but are not
488 laws of nature, the use of only three sediment sizes (sand, silt and clay), the use of only one
489 capacity transport equation for bedload estimates in all rivers, a simplified dam operation
490 scheme in the hydrological component, the adoption of a single value for the Manning
491 coefficient, and the non-inclusion of sediment sources from mining activities, which can be
492 relevant in some places.

493 Despite the limitations of the model and the associated uncertainties in sediment flux estimates,
494 it is important to note that even in situ observations can have very high uncertainties (>50%,

495 Navratil et al., 2011). More than this, for large scales (continental or global), no studies with in
496 situ sediment data have been found in the literature, and only the recent study of Dethier (et al.,
497 2022) has presented global results using remote sensing data. Thus, sediment transport models
498 have proven to be the best alternative to large-scale assessments of sediment fluxes on large
499 scales (Cohen et al., 2014, 2013; Fagundes et al., 2021; Pelletier, 2012; Syvitski et al., 2005).
500 These models also have the advantage of providing information that makes detailed spatial and
501 temporal analyses of what is happening in the landscape possible, and also intercomparisons
502 between different geographic and climatic regions. More details about the model performance
503 are discussed in the Supporting Information S1 - Text S1.

504 **4.2 Continental analysis in time and space**

505 The MGB-SED AS model has performed well in simulating sediment fluxes previously (Fagundes
506 et al., 2021), and in this study further improvements have been achieved (section 4.1).
507 Nevertheless, the presented results have uncertainties, which are not simple to quantify.
508 Therefore, the results presented here, especially those that present absolute values, should be
509 regarded with caution.

510 Our analysis indicates that 51% of the main SA rivers have shown statistically significant changes
511 in simulated sediment transport over the last 36 years (1984–2019). In 36% of the large rivers
512 evaluated (Table 1), changes were directly caused by human activities such as deforestation and
513 river damming, while precipitation alteration has driven changes in 15% of them. Absolute
514 changes in annual sediment transport above 10% were observed in 14 of the 39 main SA rivers.
515 Sediment flow increases were more frequent in the Amazon Basin rivers. By contrast, decreases
516 were detected in the northeast and southeast portions of the continent (e.g., Paraná, Uruguay,
517 Tocantins, and São Francisco rivers).

River	A (km ²)	Q (m ³ /s)	QSS (Mt/year)	QST (Mt/year)	QST change (%)	Dominant Driver
-------	----------------------	--------------------------	------------------	------------------	-------------------	--------------------

518 The average simulated sediment supply from SA rivers to the oceans was 834 million tons per
519 year (Mt/year), decreasing over the analyzed period (Figure 2). From 2011 to 2019, SA delivered
520 771 Mt/year to the oceans, almost 10 % less than the 849 Mt/year delivered from 1984 to 1992
521 (Figure 3), which is a different result from a recent study (Dethier et al., 2022). Dethier et al.
522 (2022) observed sediment changes at the mouths of major rivers and concluded that in South
523 America fluxes are increasing. These different findings result from the different approaches used
524 in each study. For example, it is known that the concentration of sediments at the mouth of the
525 Amazon River tends to be higher than in upstream regions due to local processes on the estuary
526 and coast (e.g. resuspension, Fassoni-Andrade and Paiva, 2019), and not due to the increased
527 sediment load coming from the upstream region.

528 **Table 1. Long-term estimates of sediment transport, mean alterations, and dominant drivers**
529 **of changes for the main South American rivers.** A is the drainage area, Q is the water discharge,
530 QSS and QST are the suspended and total sediment discharge, respectively.

Amazon	5,927,062	199,798	325.1	405.8	-6	-
Apure	137,051	2,094	16.0	18.1	-6	-
Araguaia	387,051	6,195	6.9	11.0	-6	-
Aripuanã	147,519	4,390	0.6	1.2	18*	LULCC
Beni	119,697	2,200	81.9	83.8	0	-
Bermejo	107,526	464	25.9	27.2	-31*	Precipitation
Branco	191,221	5,832	4.7	7.1	8	-
Colorado	295,416	185	0.2	0.6	-60*	Reservoir
Grande	143,928	2,277	0.5	0.6	-33*	Reservoir
Guaporé	355,220	3,315	3.9	5.4	18*	LULCC
Guaviare	139,337	6,454	10.4	14.3	4*	Precipitation
Iriri	142,686	4,563	0.6	1.1	19*	LULCC
Japurá	270,763	15,255	11.1	20.2	7	-
Juruá	182,140	5,979	29.2	34.5	-26	-
Madeira	1,372,401	28,823	155.3	172.2	-26	-
Madre de Dios	125,756	4,082	74.5	85.3	-2	-
Magdalena	261,343	7,304	28.2	38.9	-8*	LULCC
Mamoré	236,242	3,237	62.0	64.5	-7	-
Marañón	365,659	15,262	138.0	161.0	1	-
Meta	109,518	4,003	27.8	31.9	-7	-
Negro (Amazon)	716,166	34,887	9.2	14.2	10*	Precipitation
Negro (Argentina)	113,495	834	0.2	0.6	-80	-
Orinoco	940,567	33,186	116.9	151.2	-1*	Precipitation
Paraguay	535,249	2,541	6.0	8.5	-9	-
Paraná	2,602,798	21,792	59.2	65.1	-23*	Precipitation
Paranaíba	224,199	3,426	2.2	3.2	-44*	Reservoir
Parnaíba	333,763	962	1.9	3.4	-49	-
Pilcomayo	114,123	21	25.6	25.6	-2	-

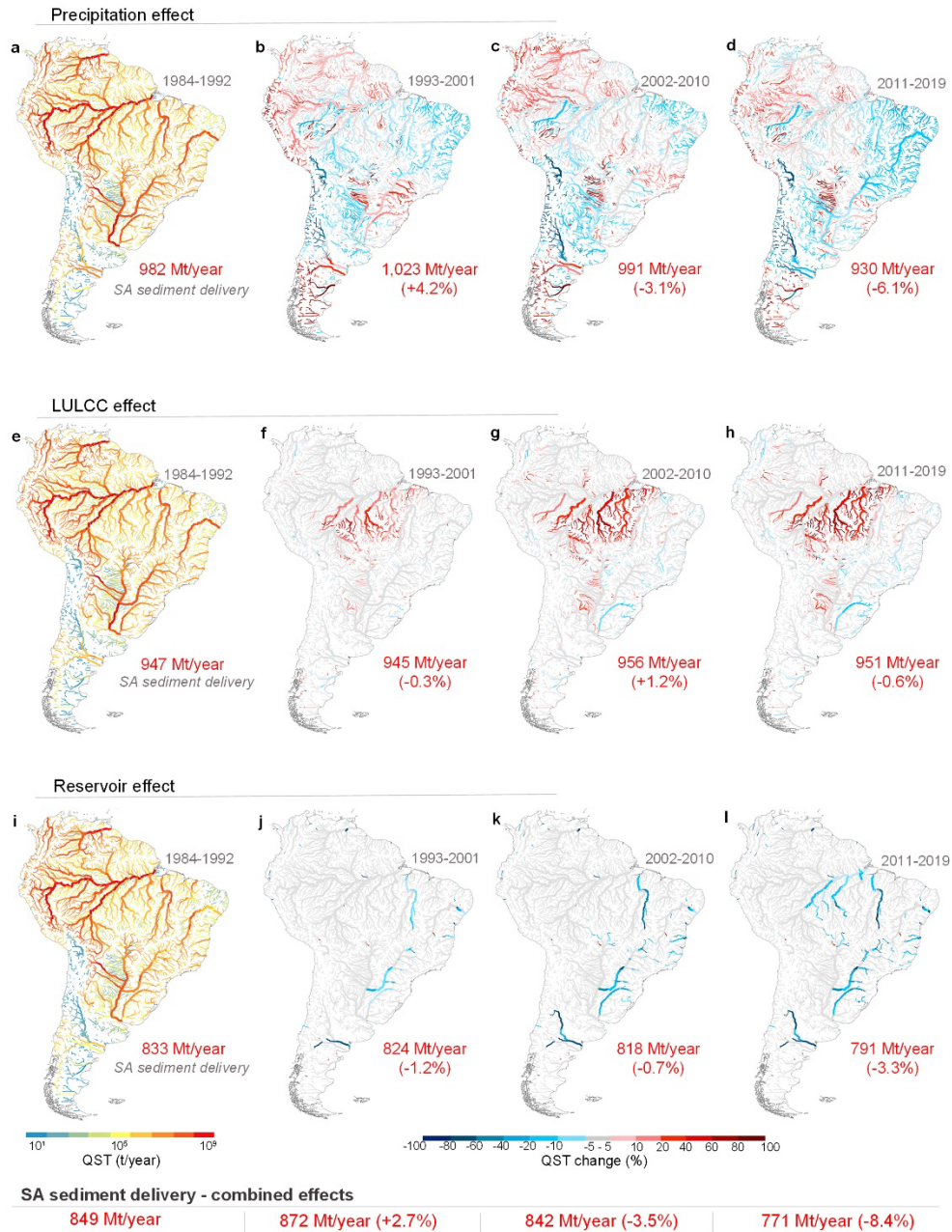
Purus	379,473	11,424	24.5	33.8	9	-
Salado	226,464	175	0.3	0.9	-12*	Reservoir
San Miguel	125,840	777	2.5	2.9	7*	LULCC
São Francisco	638,874	2,779	0.9	2.6	-42*	Precipitation
Solimões	2,219,829	90,783	249.9	304.1	1	-
Tapajós	495,396	15,260	3.4	5.8	27*	LULCC
Tocantins	774,414	13,656	5.1	6.5	-46*	Reservoir
Ucayali	353,575	9,689	102.7	119.1	-4	-
Upper Paraná	954,777	15,557	5.1	6.5	-73*	Reservoir
Uruguay	267,152	7,172	4.0	4.0	-49*	Reservoir
Xingu	514,318	13,946	2.5	4.4	1*	LULCC

531 * Statistically significant to the level of 5% from the Mann-Kendall test.

532 Amazon (405 Mt/year, 48.8%), Orinoco (151 Mt/year, 18.1%), Paraná (65 Mt/year, 7.6%) and
 533 Magdalena (39 Mt/year, 4.6%) were the main SA rivers delivering sediments to the oceans
 534 (Figure 3-a). Comparing current and baseline periods, these rivers experienced a reduction in
 535 simulated sediment flux of 5.9%, 0.7%, 23.0%, and 7.6%, respectively. Our simulations also
 536 showed that sediment delivery to the South and North Atlantic Oceans were reduced by 26.0%
 537 and 4.7%, respectively, close to the sediment delivery reductions of the Paraná (23.0%) and
 538 Amazon (5.9%) rivers (Figure 3). The -5.0% change (Figure 3-b) in sediment supply to the
 539 Caribbean (69 Mt/year, 31.3%) is mainly associated with changes in the Magdalena River
 540 sediment flows.

541 Precipitation was the main driver responsible for reducing total simulated sediment discharge
 542 (QST) in SA rivers (Figure 2). For instance, we estimated a 6.1% decrease in the sediment
 543 delivery to the oceans for the 2011–2019 period when considering only the effect of
 544 precipitation (Fig 1-A.4). The variable nature of precipitation over time showed that the climate

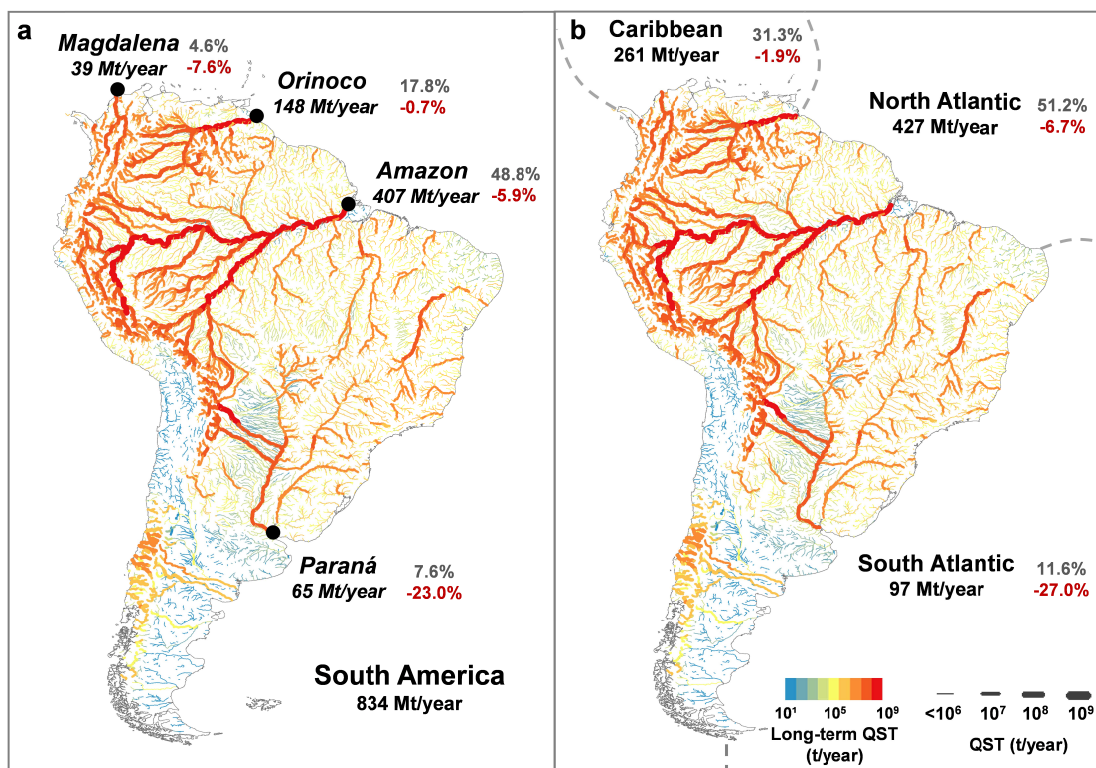
545 driver has a widespread and important impact on sediment flux changes over large portions of
 546 SA.



547

548 **Figure 2. Temporal changes in sediment fluxes in South American rivers between 1984–2019.**
 549 Maps show the QST and their changes (%) considering the isolated effect of precipitation
 550 changes (a–d), land use and land cover changes (LULCC, e–h), and existing reservoirs (i–l). Maps
 551 a, e, and i show QST values for the baseline period (1984–1992). The other maps present the
 552 sediment flow changes compared with the baseline period. Numbers in red indicate the average

558 sediment delivery from South America (SA) to the oceans in each period. Percentage values
 559 indicate the increase or decrease of sediment delivery compared with the previous period.
 560 These values are presented at the bottom (SA sediment delivery - combined effects) for the
 561 combined effect of each driver, i.e., when simulations were performed considering the synergic
 562 effect of precipitation, LULCC, and reservoirs on sediment flows.

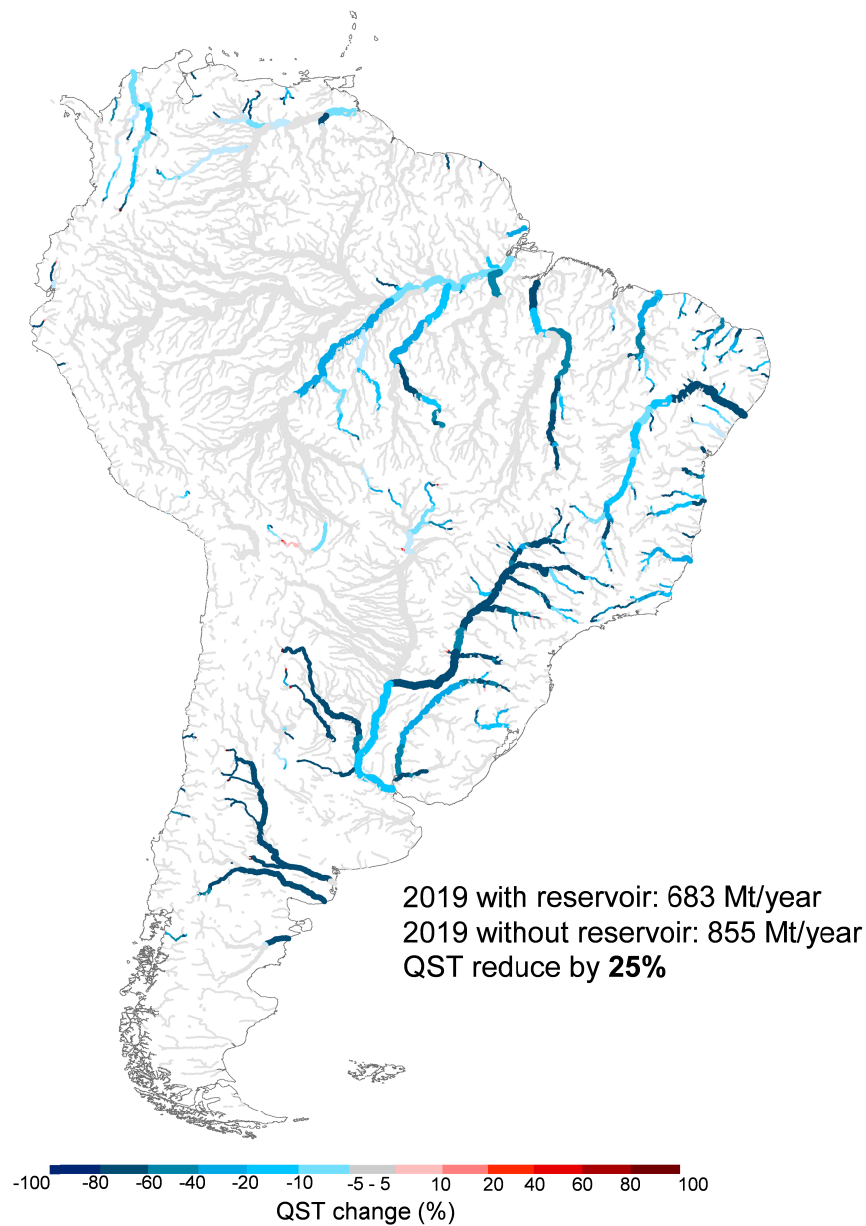


559 **Figure 3. Long-term average of total simulated sediment discharge (QST) and the impact in**
 565 **the supply to the Caribbean, North and South Atlantic oceans. a, Main rivers responsible for**
 566 **the sediment supply to the oceans. b, Amount of sediment load reaching the oceans. Gray**
 567 **numbers indicate the relative percentage of the sediment load in comparison with the total**
 568 **reaching the oceans. Red numbers indicate the relative reduction in 2011-2019 in comparison**
 569 **with 1984-1992.**
 570

572 By contrast, LULCC resulted in local but more substantial effects, with several rivers showing
 573 simulated QST changes above 80% (Figure 2-h). In addition, LULCC effects were progressive over
 574 time, and the Amazon arc of the deforestation region is the main affected area (Figure 2). This
 575 region has been deforested (1,424 ha/year, INPE - Instituto Nacional de Pesquisas Espaciais,
 576 2021) for livestock, soybean planting, and other crops (Song et al., 2021, 2018; Zalles et al.,
 577 2021). Since 1984, we observed that deforestation mostly increased the sediment flux in some
 578 Amazon sub-basins such as Juruá, Japurá, Magdalena and Branco ones, as well as along the

572 headwaters of Magdalena and Orinoco rivers (Figure 2). At the same time, more significant
573 reforestation (natural or non-natural) was observed in the Uruguay River basin, in the
574 headwaters of the Upper Paraná, São Francisco, and in some small rivers on the right bank of
575 the Paraguay River (Figure 2).

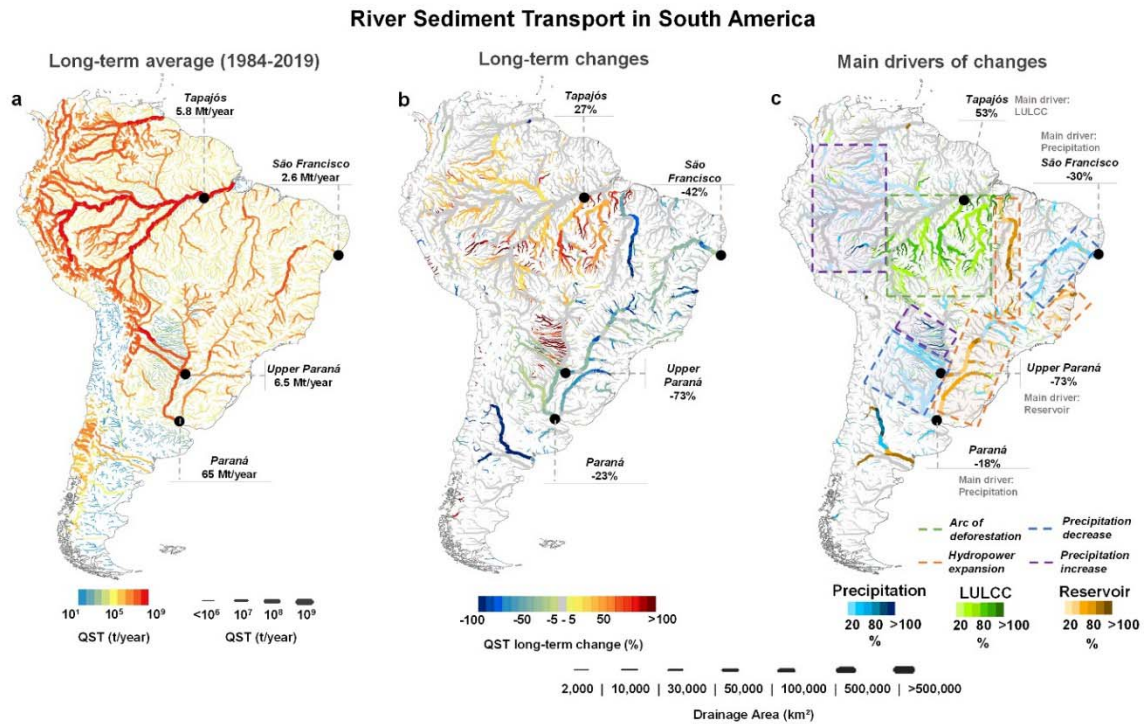
576 The effect of reservoirs was cumulative along the rivers, and greater reservoir storage capacity
577 caused more sediment retention. Sediment modeling show that from 1984 to 2010, hydropower
578 expansion led to a greater reduction of sediment flows (as high as 80-100%) in the Tocantins,
579 Uruguay, Upper Paraná, lower São Francisco, Desaguadero, and Negro rivers (Figure 2-k). In the
580 last decade, hydropower expansion has largely affected the Amazon region (Fig 2-l), resulting in
581 a significant change in the sediment flows in this region. By comparing the current (2011–2019)
582 and baseline (1984–1992) periods, river impoundments were responsible for a 5% reduction in
583 total sediment delivery to the oceans. Several reservoirs were built for the Brazilian hydropower
584 expansion, especially after its energy crisis at the beginning of the 21st century. However, many
585 dams existed in SA rivers before 1984 (Figure 1). We found a 25% reduction in sediment delivery
586 to the oceans caused by the reservoirs operating in 2019 compared with a scenario without
587 reservoirs (Figure 4). It is well known that sediment trapping in reservoir lakes can induce
588 downstream sediment erosion, but in general, the sediment volume trapped upstream greatly
589 overcomes the sediment volume eroded in downstream.



591
595 **Figure 4. QST change due to reservoir effect considering the year of 2019.** Two simulations
596 were performed: one with presence and other with absence of the 234 large reservoirs presented
597 in Extended Data Figure 1. These changes indicate not only the effect of reservoir in the
598 simulated period but also those one existing before 1984.

598 The main hotspots for simulated QST increases driven by LULCC and precipitation were in the
599 Amazon region (Figure 5). These sediment flow disturbances can require more fertilizers
500 (Borrelli et al., 2017) for food production, affecting the meander migration and generating social

598 and economic damage to riverine communities (Nagel et al., 2022). Increases in Amazon
 599 sediment flows can also be accompanied by higher mercury concentrations in rivers (Benefice et
 600 al., 2010; Webb et al., 2004; Yokoo et al., 2003), wetlands (Roulet et al., 2001) and fishes (Lino et
 601 al., 2019). These increases can be related to changes in the neurobehavioral capacities of adults
 602 observed in parts of Brazil, Ecuador, and Bolivia (Benefice et al., 2010; Webb et al., 2004; Yokoo
 603 et al., 2003).



604
 605 **Figure 5. Spatial overview of trends, magnitude, and main drivers of changes in sediment**
 606 **transport of South American rivers between 1984-2019. a)** map of the long-term average of
 607 total simulated sediment discharge (QST) considering the precipitation and human-induced
 608 changes by land use and land cover changes (LULCC) and reservoirs constructions. **b)** Statistically
 609 significant QST long-term changes to the level of 5% considering the Mann Kendall test (M-K
 610 test). **c)** Magnitude of sediment flow changes considering the main driver (precipitation, LULCC,
 611 or reservoir) in each river reach. Hotspots of changes are highlighted in rectangles. For example,
 612 it is observed that Tapajós River transported 5.8 Mt/year on average from 1984-2019, with an
 613 increasing trend of 27%, in which the LULCC (main) driver was responsible for an increase of
 614 53%.

615 Over time, the implementation of many reservoirs caused substantial simulated QST reductions
 616 (> 50%) in the Tocantins, Upper Paraná, Uruguay, and Lower São Francisco rivers (Figure 5-c).

617 Ecological and geomorphological implications have already been reported for some of these
618 rivers (Bandeira et al., 2013; da Silva et al., 2020; Maavara et al., 2015). Lower sediment supply
619 to downstream reservoirs can lead to the loss of riparian vegetation, affecting the water quality,
620 local biodiversity (Naiman et al., 1993), and other wetland vegetation species (Swanson and
621 Bohlman, 2021). Reduced sediment flows can also lead to fewer nutrients and decreased fishery
622 yields, as reported for the São Francisco (Cavali et al., 2020) and Paraná (Maavara et al., 2015)
623 rivers. Hydropower expansion has recently reached the Amazon region, resulting in a
624 statistically significant change in sediment flows. By comparing pre- and post-construction of
625 Santo Antônio and Jirau dams, we estimated a 43% decline in the Madeira River's QST. This
626 remarkable change affected the Amazon River, which experienced a 19% reduction in sediment
627 load over the same period. The coastal region between the mouths of the Amazon and Orinoco
628 rivers is the largest mud beach complex on Earth (Anthony et al., 2014) and may be seriously
629 affected by substantial reductions in sediment supply by Amazon River (Forsberg et al., 2017;
630 Latrubesse et al., 2017). This reduction could also affect the ability of mangroves to act as a
631 carbon sink. These forests account for approximately 10–15% of total carbon sequestration
632 while covering only around 0.5% of the total global coastal area (Ezcurra et al., 2019).

633 Regarding the impacts on simulated QST from precipitation decreases, the most significant
634 changes were found in the Bermejo River (-31%). This river provides approximately 90% of the
635 Lower Paraná sediment load (Amsler and Drago, 2009), playing a major role in maintaining its
636 ecosystems (Thorp et al., 2006). Climate change projections (Figure S1 - Supporting Information
637 S1) suggest that the Bermejo River will likely experience average precipitation and river
638 discharge reductions in the future. Consequently, the sediment supply to the Lower Paraná
639 River is expected to decline, increasing the vulnerability of the ecosystems that depend on it.

640 **4.3 Implications for the ecosystem, water, and land management**

641 When sediment flows are changing, other aspects of the environment can also be affected. In
642 South America, planned reservoirs (Figure S1 - Supporting Information S1) are particularly
643 concerning, especially those in the Pantanal and Amazon basin. Even if only some of them are
644 built, irreversible environmental consequences could occur (Forsberg et al., 2017). Sediments
645 from uplands carried to the Pantanal wetlands support geomorphological dynamics, wildlife
646 habitats, and biological productivity. However, existing reservoirs have reduced the sediment
647 supply by around 20% in these environments (Fantin-Cruz et al., 2020 and Figure 5). In addition,
648 Andean reservoirs can dramatically change the sediment and nutrient inflows to the Amazon
649 rivers and floodplains and the North Atlantic Ocean. An earlier study showed that six planned
650 dams accounting for only 7% of the total drainage area of the Amazon Basin could reduce the
651 basin-wide sediment supply by 64% (Forsberg et al., 2017).

652 Both increasing changes in simulated QST due to LULCC or precipitation changes in SA require
653 measures to minimize their impacts. From our results, hotspots include the Amazon, where
654 efforts should focus on reducing deforestation. However, the Brazilian Cerrado, Caatinga,
655 Atlantic Rainforest, and Pampa biomes were also severely degraded in the past and would
656 benefit significantly from erosion control practices. Our results can assist in the delineation of
657 ecosystem restoration strategies by identifying the main areas needing recovery (Zalles et al.,
658 2021), through policies such as payment for ecosystem services, for example (Latrubesse et al.,
659 2019; Song et al., 2018). Sustainable agriculture by farmers must be encouraged, providing
660 practices aimed at soil erosion reduction and improving both terrestrial and aquatic ecosystems
661 quality (Borrelli et al., 2017). Concerning mercury impacts associated with deforestation,
662 consider that (i) Brazilian Amazon riverine populations have a per capita fish consumption of up

663 to 94 kg/year, which is 5.8 times the world average (Isaac and de Almeida, 2011), and (ii) our
664 results showed that QST increase rates reached more than 80%. Therefore, the creation of
665 programs and actions to monitor fishes and prevent damage to the health of the riverine
666 population, such as providing solutions and better diet alternatives (Benefice et al., 2010), is also
667 important.

668 Although dams can cause several negative impacts on sediment flows and ecosystems, they also
669 have contributed to worldwide water and energy security, supporting economic and social
670 development (Hogeboom et al., 2018; Tilmant et al., 2014). In 2018, reservoirs used for
671 hydropower generation, irrigation, industrial and domestic water supply, flood protection,
672 fishing, and recreation were valued at US\$265 billion per year (Hogeboom et al., 2018). Because
673 of these factors, trade-offs and the adoption of sustainable management practices in reservoir
674 operation are essential (Best, 2019), including for major areas requiring new dam construction,
675 such as the Amazon and Pantanal (Randle et al., 2021). Such practices would permit sediment
676 passage through reservoirs to provide environmental benefits (Randle et al., 2021) and minimize
677 environmental impacts.

678 5 Conclusions

679 Sediment flow changes in SA induced by human activities such as deforestation and river
680 damming are a consequence of demands from local populations and other. Both increases and
681 decreases in sediment flows can be problematic for the environment and society because each
682 ecosystem is unique. Thus, in this study we aimed to comprehend the spatiotemporal changes
683 in sediment fluxes in SA over the last 36 years (1984-2019). We found that 51% of the main SA
684 rivers experienced statistically significant changes in simulated sediment transport over this

685 period, with 36% due to Amazon deforestation and river damming and 15% due to precipitation
686 changes. We also estimated a 10% reduction in the average sediment delivery to the oceans.

687 Amazon, Orinoco, Paraná and Magdalena were the main SA rivers delivering sediments to the
688 oceans, and these rivers experienced a reduction in simulated sediment flux of 5.9%, 0.7%,
689 23.0%, and 7.6%, respectively. Precipitation was the main driver responsible for reducing total
690 simulated sediment discharge (QST) in SA rivers. By contrast, LULCC resulted in local but more
691 substantial effects, with several rivers showing simulated QST changes above 80%. Similarly, to
692 LULCC, hydropower expansion led to a greater reduction of sediment flows (as high as 80-100%)
693 in the Tocantins, Uruguay, Upper Paraná, lower São Francisco, Desaguadero, and Negro rivers.
694 Our results of simulation also show that Amazon region is the most affected one due to
695 deforestation, and, especially in the last decade, also by reservoirs.

696 Our study is the first to provide a thorough and consistent analysis of the synergistic effects of
697 LULCC, river damming, and precipitation change on sediment flows for the entire SA continent
698 from 1984 to 2019. Our modeling outputs provide unprecedented information about the status
699 of sediment dynamics in SA, and a means to develop evidence-based strategies and
700 transboundary policies related to continental-wide sediment dynamics and the conservation
701 and restoration of ecosystems. This understanding of the evolution of sediment flow changes
702 across space and time can help mitigate impacts on people and nature, based on our
703 identification of the most sediment-affected regions. The approach used here can also be useful
704 as described next for applications in other locations. Furthermore, the findings and data
705 provided in this study may be useful in future investigations of carbon fluxes, nutrient transport,
706 biological productivity, human food and energy safety, and other studies related to ecosystem
707 maintenance and soil conservation.

708 The MGB-SED AS model has shown ability to properly simulate sediment fluxes in several sites
709 of South America. However, large-scale modeling is not free of uncertainties, which requires
710 that the results and conclusions be understood from this perspective. In the future, we intend to
711 perform sensitivity/uncertainties analyses to improve our knowledge about continental
712 sediment modeling, which also constitutes part of our continental modeling research agenda,
713 started with the work of Siqueira et al. (2018). Future works could also use different methods
714 and approaches to represent other processes like gully and lateral erosions; different particle
715 sizes distribution; new schemes for dam operation. In addition, the model could be updated and
716 re-calibrated using new databases of soil, land use, climate and precipitation data.

717 Acknowledgments

718 H.O.F. and F.M.F. thanks the Brazilian CNPq (Conselho Nacional de Desenvolvimento Científico e
719 Tecnológico) for supporting this research under the Grants Number 167867/2018-0 and
720 305636/2019-7. P.B. was funded by the EcoSSoil Project, Korea Environmental Industry &
721 Technology Institute (KEITI), Korea (Grant No. 2019002820004). This study was financed in part
722 by the Coordenação de Aperfeiçoamento de Pessoal de Nível Superior - Brasil (CAPES) - Finance
723 Code 001.

724 Data availability

725 Data supporting the findings of this study are available in the references cited in the main text,
726 methods, and Supporting Information S1. Also, any data can be provided from the
727 corresponding author upon reasonable request. Simulated Suspended Sediment Discharge for
728 South America Rivers (MGB-SED AS) - V2.0 dataset is available in:
729 doi.org/10.17632/ncr6d42tx5.1. This dataset provides both annual long-term average and daily

730 simulated data. More information and datasets can be found in

731 <https://www.ufrgs.br/samewater/>.

732

733 Code availability

734 The source code of the MGB-SED AS model is available at

735 <https://www.ufrgs.br/samewater/produtos/south-america-sediment-model/>

736 6 References

737 Alarcón, J.J., Szupiany, R., Montagnini, M.D., Gaudin, H., Prendes, H.H., Amsler, M.L., 2003.
738 Evaluación del transporte de sedimentos en el tramo medio del Río Paraná, in: Primer
739 Simposio Regional Sobre Hidráulica de Ríos. Ezeiza.

740 Albert, J.S., Destouni, G., Duke-Sylvester, S.M., Magurran, A.E., Oberdorff, T., Reis, R.E.,
741 Winemiller, K.O., Ripple, W.J., 2021. Scientists' warning to humanity on the freshwater
742 biodiversity crisis. *Ambio* 50, 85–94. <https://doi.org/10.1007/s13280-020-01318-8>

743 Almagro, A., Oliveira, P.T.S., Nearing, M.A., Hagemann, S., 2017. Projected climate change
744 impacts in rainfall erosivity over Brazil. *Sci Rep* 7, 1–12. <https://doi.org/10.1038/s41598-017-08298-y>

746 Amsler, M.L., Drago, E.C., 2009. A review of the suspended sediment budget at the confluence
747 of the Paraná and Paraguay Rivers. *Hydrological Processes: An International Journal* 23,
748 3230–3235. <https://doi.org/10.1002/hyp>

749 Andreadis, K.M., Schumann, G.J.P., Pavelsky, T., 2013. A simple global river bankfull width and
750 depth database. *Water Resources Research*.

751 Anthony, E.J., Gardel, A., Gratiot, N., 2014. Fluvial sediment supply, mud banks, cheniers and the
752 morphodynamics of the coast of South America between the Amazon and Orinoco river
753 mouths. *Geol Soc Spec Publ* 388, 533–560. <https://doi.org/10.1144/SP388.8>

754 Bandeira, J.V., Farias, E. de G.G., Lorenzetti, J.A., Salim, L.H., 2013. Resposta morfológica da foz
755 do rio São Francisco, devido à retenção de sedimentos nos reservatórios. *Vetor* 23, 5–17.

756 Barbarossa, V., Schmitt, R.J.P., Huijbregts, M.A.J., Zarfl, C., King, H., Schipper, A.M., 2020.
757 Impacts of current and future large dams on the geographic range connectivity of
758 freshwater fish worldwide. *Proc Natl Acad Sci U S A* 117, 3648–3655.
759 <https://doi.org/10.1073/pnas.1912776117>

- 760 Bates, P.D., Horritt, M.S., Fewtrell, T.J., 2010. A simple inertial formulation of the shallow water
761 equations for efficient two-dimensional flood inundation modelling. *J Hydrol (Amst)* 387,
762 33–45. <https://doi.org/10.1016/j.jhydrol.2010.03.027>
- 763 Beck, H.E., van Dijk, A.I.J.M., de Roo, A., Dutra, E., Fink, G., Orth, R., Schellekens, J., 2017. Global
764 evaluation of runoff from 10 state-of-the-art hydrological models. *Hydrol Earth Syst Sci* 21,
765 2881–2903.
- 766 Beighley, R.E., Gummadi, V., 2011. Developing channel and floodplain dimensions with limited
767 data: A case study in the Amazon Basin. *Earth Surf Process Landf* 36, 1059–1071.
- 768 Benavidez, R., Jackson, B., Maxwell, D., Norton, K., 2018. A review of the (Revised) Universal Soil
769 Loss Equation ((R)USLE): With a view to increasing its global applicability and improving soil
770 loss estimates. *Hydrol Earth Syst Sci* 22, 6059–6086. [https://doi.org/10.5194/hess-22-](https://doi.org/10.5194/hess-22-6059-2018)
771 [6059-2018](https://doi.org/10.5194/hess-22-6059-2018)
- 772 Benefice, E., Luna-Monroy, S., Lopez-Rodriguez, R., 2010. Fishing activity, health characteristics
773 and mercury exposure of Amerindian women living alongside the Beni River (Amazonian
774 Bolivia). *Int J Hyg Environ Health* 213, 458–464.
775 <https://doi.org/10.1016/j.ijheh.2010.08.010>
- 776 Best, J., 2019. Anthropogenic stresses on the world’s big rivers. *Nat Geosci* 12, 7–21.
777 <https://doi.org/10.1038/s41561-018-0262-x>
- 778 Borrelli, P., Robinson, D.A., Fleischer, L.R., Lugato, E., Ballabio, C., Alewell, C., Meusburger, K.,
779 Modugno, S., Schütt, B., Ferro, V., Bagarello, V., Oost, K. van, Montanarella, L., Panagos, P.,
780 2017. An assessment of the global impact of 21st century land use change on soil erosion.
781 *Nat Commun* 8, 1–13. <https://doi.org/10.1038/s41467-017-02142-7>
- 782 Bozkurt, D., Rondanelli, R., Garreaud, R., 2016. Impact of Warmer Eastern Tropical Pacific SST on
783 the March 2015 Atacama Floods. *American Meteorological Society* 144, 4441–4460.
784 <https://doi.org/10.1175/MWR-D-16-0041.s1>
- 785 Buarque, D.C., 2015. Simulação da geração e do transporte de sedimentos em grandes bacias:
786 estudo de caso do rio Madeira. Universidade Federal do Rio Grande do Sul, Porto Alegre,
787 Tese (Doutorado em Recursos Hídricos e Saneamento Ambiental).
- 788 Cai, W., McPhaden, M.J., Grimm, A.M., Rodrigues, R.R., Taschetto, A.S., Garreaud, R.D., Dewitte,
789 B., Poveda, G., Ham, Y.G., Santoso, A., Ng, B., Anderson, W., Wang, G., Geng, T., Jo, H.S.,
790 Marengo, J.A., Alves, L.M., Osman, M., Li, S., Wu, L., Karamperidou, C., Takahashi, K., Vera,
791 C., 2020. Climate impacts of the El Niño–Southern Oscillation on South America. *Nat Rev*
792 *Earth Environ*. <https://doi.org/10.1038/s43017-020-0040-3>
- 793 Carvalho, T.M., 2009. Avaliação do transporte de carga sedimentar no médio rio Araguaia.
794 *Geosul* 24, 147–160.
- 795 Cavali, J., Mojica, A.B., Filho, J.V.D., 2020. Percepção dos pescadores sobre as mudanças no
796 baixo rio São Francisco, in: Soares, E.C., Silva, J.V., Navas, R. (Eds.), *O Baixo São Francisco:*
797 *Características Ambientais e Sociais*. Edufal, Maceió-AL.

- 798 CNEN/CDTN - Centro de Desenvolvimento da Tecnologia Nuclear, IFNMG/Campus Januária -
799 Instituto Federal do Norte de Minas Gerais, 2020. Caracterização Qualitativa e Quantitativa
800 de Parâmetros Hídricos e Sedimentológicos da Rede de Drenagem do Rio Pandeiros. Belo
801 Horizonte.
- 802 Cohen, S., Kettner, A.J., Syvitski, J.P.M., 2014. Global suspended sediment and water discharge
803 dynamics between 1960 and 2010: Continental trends and intra-basin sensitivity. *Glob*
804 *Planet Change* 115, 44–58. <https://doi.org/10.1016/j.gloplacha.2014.01.011>
- 805 Cohen, S., Kettner, A.J., Syvitski, J.P.M., Fekete, B.M., 2013. WBMsed, a distributed global-scale
806 riverine sediment flux model: Model description and validation. *Comput Geosci* 53, 80–93.
807 <https://doi.org/10.1016/j.cageo.2011.08.011>
- 808 Collischonn, W., Allasia, D., da Silva, B.C., Tucci, C.E.M., 2007. The MGB-IPH model for large-scale
809 rainfall-runoff modelling. *Hydrological Sciences Journal* 52, 878–895.
810 <https://doi.org/10.1623/hysj.52.5.878>
- 811 Costanza, R., de Groot, R., Farberll, S., Grassot, M., Hannon, B., Limburg, K., Naeem, S., O, R. v,
812 Paruelo, J., Raskin, R.G., Suttonllll, P., 1997. The value of the world’s ecosystem services
813 and natural capital. *Nature* 387, 253–260.
814 <https://doi.org/https://doi.org/10.1038/387253a0>
- 815 da Silva, I.G., Pelicice, F.M., Rodrigues, L.C., 2020. Loss of phytoplankton functional and
816 taxonomic diversity induced by river regulation in a large tropical river. *Hydrobiologia* 847,
817 3471–3485. <https://doi.org/10.1007/s10750-020-04355-2>
- 818 Dethier, E.N., Renshaw, C.E., Magilligan, F.J., 2022. Rapid changes to global river suspended
819 sediment flux by humans. *Science (1979)* 376, 1447–1452.
- 820 Diodato, N., Filizola, N., Borrelli, P., Panagos, P., Bellocchi, G., 2020. The rise of climate-driven
821 sediment discharge in the amazonian river basin. *Atmosphere (Basel)* 11.
822 <https://doi.org/10.3390/atmos11020208>
- 823 Dissanayake, C.B., Chandrajith, R., 2009. Phosphate Mineral Fertilizers, trace metals and human
824 health. *J Natl Sci Found.* <https://doi.org/10.4038/jnsfsr.v37i3.1219>
- 825 Doetterl, S., van Oost, K., Six, J., 2012. Towards constraining the magnitude of global agricultural
826 sediment and soil organic carbon fluxes. *Earth Surf Process Landf* 37, 642–655.
827 <https://doi.org/10.1002/esp.3198>
- 828 Dunn, F.E., Darby, S.E., Nicholls, R.J., Cohen, S., Zarfl, C., Fekete, B.M., 2019. Projections of
829 declining fluvial sediment delivery to major deltas worldwide in response to climate
830 change and anthropogenic stress. *Environmental Research Letters* 14, 084034.
831 <https://doi.org/10.1088/1748-9326/ab304e>
- 832 Ezcurra, E., Barrios, E., Ezcurra, P., Ezcurra, A., Vanderplank, S., Vidal, O., Villanueva-Almanza, L.,
833 Aburto-Oropeza, O., 2019. A natural experiment reveals the impact of hydroelectric dams
834 on the estuaries of tropical rivers. *Sci. Adv* 5, 9875–9888.
835 <https://doi.org/10.1126/sciadv.aau9875>

- 836 Fagundes, H. de O., Fan, F.M., Paiva, R.C.D., 2019. Automatic calibration of a large-scale
837 sediment model using suspended sediment concentration, water quality, and remote
838 sensing data. *Brazilian Journal of Water Resources* 24, 1–18. [https://doi.org/10.1590/2318-](https://doi.org/10.1590/2318-0331.241920180127)
839 [0331.241920180127](https://doi.org/10.1590/2318-0331.241920180127)
- 840 Fagundes, H.O., Fan, F.M., Paiva, R.C.D., Siqueira, V.A., Buarque, D.C., Kornowski, L.W., Laipelt,
841 L., Collischonn, W., 2021. Sediment Flows in South America Supported by Daily Hydrologic-
842 Hydrodynamic Modeling. *Water Resour Res* 57. <https://doi.org/10.1029/2020WR027884>
- 843 Fagundes, H.O., Paiva, R.C.D., Fan, F.M., Buarque, D.C., Fassoni-Andrade, A.C., 2020. Sediment
844 modeling of a large-scale basin supported by remote sensing and in-situ observations.
845 *Catena (Amst)* 190, 104535. <https://doi.org/10.1016/j.catena.2020.104535>
- 846 Fan, F.M., Buarque, D.C., Pontes, P.R.M., Collischonn, W., 2015. Um Mapa de Unidades de
847 Resposta Hidrológica para a América do Sul. XXI Simpósio Brasileiro e Recursos Hídricos 1–
848 8.
- 849 Fan, F.M., Siqueira, V.A., Fleischmann, A.S., Brêda, J.P.F., de Paiva, R.C.D., Pontes, P.R.M.,
850 Collischonn, W., 2021a. On the discretization of river networks for large scale hydrologic-
851 hydrodynamic models. *Revista Brasileira de Recursos Hídricos* 26.
852 <https://doi.org/10.1590/2318-0331.262120200070>
- 853 Fan, F.M., Siqueira, V.A., Fleischmann, A.S., Brêda, J.P.F., de Paiva, R.C.D., Pontes, P.R.M.,
854 Collischonn, W., 2021b. On the discretization of river networks for large scale hydrologic-
855 hydrodynamic models. *Revista Brasileira de Recursos Hídricos* 26.
856 <https://doi.org/10.1590/2318-0331.262120200070>
- 857 Fantin-Cruz, I., de Oliveira, M.D., Campos, J.A., de Campos, M.M., de Souza Ribeiro, L., Mingoti,
858 R., de Souza, M.L., Pedrollo, O., Hamilton, S.K., 2020. Further Development of Small
859 Hydropower Facilities Will Significantly Reduce Sediment Transport to the Pantanal
860 Wetland of Brazil. *Front Environ Sci* 8. <https://doi.org/10.3389/fenvs.2020.577748>
- 861 FAO/UNESCO, 1974. FAO/UNESCO Soil Map of the World | Food and Agriculture Organization of
862 the United Nations [WWW Document]. FAO/UNESCO Soil Map of the World.
- 863 Fassoni-Andrade, A.C., Paiva, R.C.D. de, 2019. Mapping spatial-temporal sediment dynamics of
864 river-floodplains in the Amazon. *Remote Sens Environ* 221, 94–107.
865 <https://doi.org/10.1016/j.rse.2018.10.038>
- 866 Filho, O.S., 2016. Monitoramento hidrossedimentométrico e avaliação de métodos de cálculo de
867 descarga sólida total no rio Vacacaí Mirim (Dissertação). Universidade Federal de Santa
868 Maria, Santa Maria.
- 869 Fleischmann, A., Collischonn, W., Paiva, R., Tucci, C.E., 2019a. Modeling the role of reservoirs
870 versus floodplains on large-scale river hydrodynamics. *Natural Hazards* 99, 1075–1104.
871 <https://doi.org/10.1007/s11069-019-03797-9>
- 872 Fleischmann, A., Paiva, R., Collischonn, W., 2019b. Can regional to continental river
873 hydrodynamic models be locally relevant? A cross-scale comparison. *J Hydrol X* 3, 100027.
874 <https://doi.org/10.1016/j.hydroa.2019.100027>

- 875 Fleischmann, A., Siqueira, V., Paris, A., Collischonn, W., Paiva, R., Pontes, P., Crétaux, J.F., Bergé-
876 Nguyen, M., Biancamaria, S., Gosset, M., Calmant, S., Tanimoun, B., 2018. Modelling
877 hydrologic and hydrodynamic processes in basins with large semi-arid wetlands. *J Hydrol*
878 (Amst) 561, 943–959. <https://doi.org/10.1016/j.jhydrol.2018.04.041>
- 879 Fleischmann, A.S., Brêda, J.P.F., Passaia, O.A., Wongchuig, S.C., Fan, F.M., Paiva, R.C.D.,
880 Marques, G.F., Collischonn, W., 2021. Regional scale hydrodynamic modeling of the river-
881 floodplain-reservoir continuum. *J Hydrol (Amst)* 596.
882 <https://doi.org/10.1016/j.jhydrol.2021.126114>
- 883 Föeger, L.B., Buarque, D.C., Pontes, P.R.M., Fagundes, H. de O., Fan, F.M., 2022. Large-scale
884 sediment modeling with inertial flow routing: Assessment of Madeira river basin.
885 *Environmental Modelling and Software* 149.
886 <https://doi.org/10.1016/j.envsoft.2022.105332>
- 887 Forsberg, B.R., Melack, J.M., Dunne, T., Barthem, R.B., Goulding, M., Paiva, R.C.D., Sorribas, M.
888 v., Silva, U.L., Weisser, S., 2017. The potential impact of new Andean dams on Amazon
889 fluvial ecosystems, *PLoS ONE*. <https://doi.org/10.1371/journal.pone.0182254>
- 890 Gamaro, P.E.M., Maldonado, L.H., Castro, J.L., 2014. APLICAÇÃO DO MÉTODO DAS DUNAS PARA
891 DETERMINAÇÃO DA DESCARGA DE FUNDO NO RIO PARANÁ, in: *Anais Do XI Encontro*
892 *Nacional de Engenharia de Sedimentos*. João Pessoa.
- 893 Gamaro, P.E.M., Maldonado, L.H., Lima, K.A., 2011. AVALIAÇÃO DA CARGA DE SEDIMENTOS DE
894 FUNDO PELO MÉTODO DE DESLOCAMENTO DE DUNAS E MEDIDORES ACÚSTICOS
895 DOPPLER, in: *Anais Do XIX Simpósio Brasileiro de Recursos Hídricos*. Maceió.
- 896 Getirana, A., Peters-Lidard, C., Rodell, M., Bates, P.D., 2017. Trade-off between cost and
897 accuracy in large-scale surface water dynamic modeling. *Water Resour Res* 53, 4942–4955.
898 <https://doi.org/10.1002/2017WR020519>
- 899 González, M.H., Murgida, A.M., 2012. 7 Seasonal Summer Rainfall Prediction in Bermejo River
900 Basin in Argentina, in: Hannachi, A. (Ed.), *Climate Variability—Some Aspects, Challenges*
901 *and Prospects*. InTech, pp. 141–160.
- 902 Grill, G., Lehner, B., Thieme, M., Geenen, B., Tickner, D., Antonelli, F., Babu, S., Borrelli, P.,
903 Cheng, L., Crochetiere, H., Ehalt Macedo, H., Filgueiras, R., Goichot, M., Higgins, J., Hogan,
904 Z., Lip, B., McClain, M.E., Meng, J., Mulligan, M., Nilsson, C., Olden, J.D., Opperman, J.J.,
905 Petry, P., Reidy Liermann, C., Sáenz, L., Salinas-Rodríguez, S., Schelle, P., Schmitt, R.J.P.,
906 Snider, J., Tan, F., Tockner, K., Valdujo, P.H., van Soesbergen, A., Zarfl, C., 2019. Mapping
907 the world’s free-flowing rivers. *Nature* 569, 215–221. [https://doi.org/10.1038/s41586-019-](https://doi.org/10.1038/s41586-019-1111-9)
908 [1111-9](https://doi.org/10.1038/s41586-019-1111-9)
- 909 Hanasaki, N, Kanae, S., Oki, T., 2006. A reservoir operation scheme for global river routing
910 models. *J Hydrol (Amst)* 327, 22–41.
- 911 Hanasaki, Naota, Kanae, S., Oki, T., 2006. A reservoir operation scheme for global river routing
912 models. *J Hydrol (Amst)* 327, 22–41. <https://doi.org/10.1016/j.jhydrol.2005.11.011>

- 913 Hogeboom, R.J., Knook, L., Hoekstra, A.Y., 2018. The blue water footprint of the world's artificial
914 reservoirs for hydroelectricity, irrigation, residential and industrial water supply, flood
915 protection, fishing and recreation. *Adv Water Resour* 113, 285–294.
916 <https://doi.org/10.1016/j.advwatres.2018.01.028>
- 917 Huang, C., Zhou, Z., Teng, M., Wu, C., Wang, P., 2020. Effects of climate, land use and land cover
918 changes on soil loss in the Three Gorges Reservoir area, China. *Geography and*
919 *Sustainability* 1, 200–208. <https://doi.org/10.1016/j.geosus.2020.08.001>
- 920 INPE - Instituto Nacional de Pesquisas Espaciais, 2021. TerraBrasilis. PRODES (Desmatamento).
921 Taxas de desmatamento acumulado.
922 <http://www.obt.inpe.br/OBT/assuntos/programas/amazonia/prodes/citacoes-ao-prodes>.
- 923 Isaac, V.J., de Almeida, M.C., 2011. El consumo de pescado en La Amazonía Brasileña. Rome.
- 924 Julien, P.Y., 2010. *Erosion and Sedimentation*, Second. ed. Cambridge University Press, New
925 York.
- 926 Kemppinen, K.M.S., Collins, P.M., Hole, D.G., Wolf, C., Ripple, W.J., Gerber, L.R., 2020. Global
927 reforestation and biodiversity conservation. *Conservation Biology* 34, 1221–1228.
928 <https://doi.org/10.1111/cobi.13478>
- 929 Kendall, M.G., Gibbons, J.D., 1975. *Rank correlation methods*. Griffin, London.
- 930 Kouwen, N., Soulis, E.D., Pietroniro, A., Donald, J., HARRINGTON; R. A, 1993. Grouped Response
931 Units for Distributed Hydrologic Modeling. *J Water Resour Plan Manag* 119, 289–305.
- 932 Latosinski, F.G., Szupiany, R.N., Guerrero, M., Amsler, M.L., Vionnet, C., 2017. The ADCP's
933 bottom track capability for bedload prediction: Evidence on method reliability from sandy
934 river applications. *Flow Measurement and Instrumentation* 54, 124–135.
935 <https://doi.org/10.1016/j.flowmeasinst.2017.01.005>
- 936 Latrubesse, E.M., Amsler, M.L., de Morais, R.P., Aquino, S., 2009. The geomorphologic response
937 of a large pristine alluvial river to tremendous deforestation in the South American tropics:
938 The case of the Araguaia River. *Geomorphology* 113, 239–252.
939 <https://doi.org/10.1016/j.geomorph.2009.03.014>
- 940 Latrubesse, E.M., Arima, E., Ferreira, M.E., Nogueira, S.H., Wittmann, F., Dias, M.S., Dagosta,
941 F.C.P., Bayer, M., 2019. Fostering water resource governance and conservation in the
942 Brazilian Cerrado biome. *Conserv Sci Pract* 1. <https://doi.org/10.1111/csp2.77>
- 943 Latrubesse, E.M., Arima, E.Y., Dunne, T., Park, E., Baker, V.R., D'Horta, F.M., Wight, C.,
944 Wittmann, F., Zuanon, J., Baker, P.A., Ribas, C.C., Norgaard, R.B., Filizola, N., Ansar, A.,
945 Flyvbjerg, B., Stevaux, J.C., 2017. Damming the rivers of the Amazon basin. *Nature* 546,
946 363–369. <https://doi.org/10.1038/nature22333>
- 947 Latrubesse, E.M., Stevaux, J.C., Sinha, R., 2005. Tropical rivers. *Geomorphology* 70, 187–206.
948 <https://doi.org/10.1016/j.geomorph.2005.02.005>

- 949 Lehner, B., Verdin, K., Jarvis, A., 2008. New global hydrography derived from spaceborne
950 elevation data. *Eos (Washington DC)* 89, 93–94.
951 <https://doi.org/https://doi.org/10.1029/2008EO100001>
- 952 Li, L., Ni, J., Chang, F., Yue, Y., Frolova, N., Magritsky, D., Borthwick, A.G.L., Ciais, P., Wang, Y.,
953 Zheng, C., Walling, D.E., 2020. Global trends in water and sediment fluxes of the world's
954 large rivers. *Sci Bull (Beijing)* 65, 62–69. <https://doi.org/10.1016/j.scib.2019.09.012>
- 955 Lino, A.S., Kasper, D., Guida, Y.S., Thomaz, J.R., Malm, O., 2019. Total and methyl mercury
956 distribution in water, sediment, plankton and fish along the Tapajós River basin in the
957 Brazilian Amazon. *Chemosphere* 235, 690–700.
958 <https://doi.org/10.1016/j.chemosphere.2019.06.212>
- 959 Maavara, T., Parsons, C.T., Ridenour, C., Stojanovic, S., Dürr, H.H., Powley, H.R., van Cappellen,
960 P., 2015. Global phosphorus retention by river damming. *Proc Natl Acad Sci U S A* 112,
961 15603–15608. <https://doi.org/10.1073/pnas.1511797112>
- 962 Macklin, M.G., Lewin, J., 2019. River stresses in anthropogenic times: Large-scale global patterns
963 and extended environmental timelines. *Prog Phys Geogr* 43, 3–23.
964 <https://doi.org/10.1177/0309133318803013>
- 965 Marengo, J.A., Galdos, M. v., Challinor, A., Cunha, A.P., Marin, F.R., Vianna, M. dos S., Alvala,
966 R.C.S., Alves, L.M., Moraes, O.L., Bender, F., 2022. Drought in Northeast Brazil: A review of
967 agricultural and policy adaptation options for food security. *Climate Resilience and*
968 *Sustainability* 1. <https://doi.org/10.1002/cli2.17>
- 969 Martins, D.P., Bravard, J.-P., Stevaux, J.C., 2009. Dynamics of water flow and sediments in the
970 Upper Paraná River between Porto Primavera and Itaipu Dams, Brazil. *Latin American*
971 *Journal of Sedimentology and Basin Analysis* 16, 111–118.
- 972 Martins, D.P., Stevaux, J.C., 2005. Formas de leito e transporte de carga de fundo do Alto Rio
973 Paraná. *Revista Brasileira de Geomorfologia* 6, 43–50.
- 974 Montanarella, L., Pennock, D.J., McKenzie, N., Badraoui, M., Chude, V., Baptista, I., Mamo, T.,
975 Yemefack, M., Aulakh, M.S., Yagi, K., Hong, S.Y., Vijarnsorn, P., Zhang, G.L., Arrouays, D.,
976 Black, H., Krasilnikov, P., Sobocká, J., Alegre, J., Henriquez, C.R., Mendonça-Santos, M. de
977 L., Taboada, M., Espinosa-Victoria, D., AlShankiti, A., AlaviPanah, S.K., Mustafa Elsheikh,
978 E.A. el, Hempel, J., Arbestain, M.C., Nachtergaele, F., Vargas, R., 2016. World's soils are
979 under threat. *SOIL* 2, 79–82. <https://doi.org/10.5194/soil-2-79-2016>
- 980 Mulligan, M., van Soesbergen, A., Sáenz, L., 2020. GOODD, a global dataset of more than 38,000
981 georeferenced dams. *Sci Data* 7. <https://doi.org/10.1038/s41597-020-0362-5>
- 982 Nagel, G.W., Novo, E.M.L. de M., Martins, V.S., Campos-Silva, J.V., Barbosa, C.C.F., Bonnet, M.P.,
983 2022. Impacts of meander migration on the Amazon riverine communities using Landsat
984 time series and cloud computing. *Science of the Total Environment* 806.
985 <https://doi.org/10.1016/j.scitotenv.2021.150449>
- 986 Naiman, R.J., Decamps, H., Pollock, M., 1993. The Role of Riparian Corridors in Maintaining
987 Regional Biodiversity. *Ecological Applications* 3, 209–212.

- 988 Nash, J.E., Sutcliffe, J. v, 1970. River Flow Forecasting Through Conceptual Models Part I-a
989 Discussion of Principles. *J Hydrol (Amst)* 10, 282–290. [https://doi.org/10.1016/0022-](https://doi.org/10.1016/0022-1694(70)90255-6)
990 1694(70)90255-6
- 991 Navratil, O., Esteves, M., Legout, C., Gratiot, N., Nemery, J., Willmore, S., Grangeon, T., 2011.
992 Global uncertainty analysis of suspended sediment monitoring using turbidimeter in a
993 small mountainous river catchment. *J Hydrol (Amst)* 398, 246–259.
994 <https://doi.org/10.1016/j.jhydrol.2010.12.025>
- 995 New, M., Lister, D., Hulme, M., Makin, I., 2002. A high-resolution data set of surface climate over
996 global land areas. *Clim Res* 21, 1–25.
- 997 Oestreicher, J.S., Lucotte, M., Moingt, M., Bélanger, É., Rozon, C., Davidson, R., Mertens, F.,
998 Romaña, C.A., 2017. Environmental and Anthropogenic Factors Influencing Mercury
999 Dynamics During the Past Century in Floodplain Lakes of the Tapajós River, Brazilian
1000 Amazon. *Arch Environ Contam Toxicol* 72, 11–30. [https://doi.org/10.1007/s00244-016-](https://doi.org/10.1007/s00244-016-0325-1)
1001 0325-1
- 1002 O’Loughlin, F.E., Paiva, R.C.D., Durand, M., Alsdorf, D.E., Bates, P.D., 2016. A multi-sensor
1003 approach towards a global vegetation corrected SRTM DEM product. *Remote Sens Environ*
1004 182, 49–59.
- 1005 Paiva, J.B.D. de, 1988. Avaliação dos modelos matemáticos para o cálculo do transporte de
1006 sedimentos em rios. Universidade de São Paulo, São Carlos.
- 1007 Paiva, J.B.D. de, Noal, A.Á., Alves, C.B., Rizzardi, A.S., Schons, C.A., Cechin, G., Libraga, J., 2011.
1008 Caracterização hidrossedimentométrica da bacia hidrográfica do rio Vacacaí Mirim, com
1009 base em dados medidos de vazão e sedimentos, in: *Anais Do XX Simposio Brasileiro de*
1010 *Recursos Hídricos*. Bento Gonçalves.
- 1011 Paiva, L.E.D. de, 2007. A influência do diâmetro representativo do material de leito nas fórmulas
1012 de cálculo do transporte de sedimentos em escoamentos com superfície livre (Tese).
1013 Universidade Estadual de Campinas, Campinas.
- 1014 Paiva, R.C.D., Buarque, D.C., Collischonn, W., Bonnet, M.P., Frappart, F., Calmant, S., Bulh??es
1015 Mendes, C.A., 2013. Large-scale hydrologic and hydrodynamic modeling of the Amazon
1016 River basin. *Water Resour Res* 49, 1226–1243. <https://doi.org/10.1002/wrcr.20067>
- 1017 Paiva, R.C.D., Collischonn, W., Tucci, C.E.M., 2011. Large scale hydrologic and hydrodynamic
1018 modeling using limited data and a GIS based approach. *J Hydrol (Amst)* 406, 170–181.
1019 <https://doi.org/10.1016/j.jhydrol.2011.06.007>
- 1020 Pelletier, J.D., 2012. A spatially distributed model for the long-term suspended sediment
1021 discharge and delivery ratio of drainage basins. *J Geophys Res Earth Surf* 117, 1–15.
1022 <https://doi.org/10.1029/2011JF002129>
- 1023 Pontes, P.R.M., 2016. Modelagem hidrológica e hidrodinâmica integrada da bacia do Prata.
1024 Universidade Federal do Rio Grande do Sul.

- 1025 Pontes, P.R.M., Fan, F.M., Fleischmann, A.S., Paiva, R.C.D., Buarque, D.C., Siqueira, V.A., Jardim,
1026 P.F., Sorribas, M.V., Collischonn, W., 2017. MGB-IPH model for hydrological and hydraulic
1027 simulation of large floodplain river systems coupled with open source GIS. *Environmental*
1028 *Modelling and Software* 94, 1–20.
- 1029 Quinton, J.N., Govers, G., van Oost, K., Bardgett, R.D., 2010. The impact of agricultural soil
1030 erosion on biogeochemical cycling. *Nat Geosci* 3, 311–314.
1031 <https://doi.org/10.1038/ngeo838>
- 1032 Randle, T.J., Morris, G.L., Tullios, D.D., Weirich, F.H., Kondolf, G.M., Moriasi, D.N., Annandale,
1033 G.W., Fripp, J., Minear, J.T., Wegner, D.L., 2021. Sustaining United States reservoir storage
1034 capacity: Need for a new paradigm. *J Hydrol (Amst)*.
1035 <https://doi.org/10.1016/j.jhydrol.2021.126686>
- 1036 Rizzardi, A.S., 2013. Avaliação e caracterização dos sedimentos transportados no rio Vacacaí
1037 Mirim (Dissertação). Universidade Federal de Santa Maria, Santa Maria.
- 1038 Roulet, M., Guimarães, J.R.D., Lucotte, M., 2001. Methylmercury production and accumulation
1039 in sediments and soils of an amazonian floodplain-effect of seasonal inundation. *Water Air*
1040 *Soil Pollut* 128, 41–60.
- 1041 Sartori, M., Philippidis, G., Ferrari, E., Borrelli, P., Lugato, E., Montanarella, L., Panagos, P., 2019.
1042 A linkage between the biophysical and the economic: Assessing the global market impacts
1043 of soil erosion. *Land use policy* 86, 299–312.
1044 <https://doi.org/10.1016/j.landusepol.2019.05.014>
- 1045 Shin, S., Pokhrel, Y., Miguez-Macho, G., 2019. High-resolution modeling of reservoir release and
1046 storage dynamics at the continental scale. *Water Resources Research* 55, 787–810.
- 1047 Shuttleworth, W.J., 1993. Evaporation, in: Maidment, D. (Ed.), *Handbook of Hydrology*. McGraw-
1048 Hill, New York.
- 1049 Siqueira, V.A., Paiva, R.C.D., Fleischmann, A.S., Fan, F.M., Ruhoff, A.L., Pontes, P.R.M., Paris, A.,
1050 Calmant, S., Collischonn, W., 2018. Toward continental hydrologic-hydrodynamic modeling
1051 in South America. *Hydrol Earth Syst Sci* 22, 4815–4842. [https://doi.org/10.5194/hess-22-](https://doi.org/10.5194/hess-22-4815-2018)
1052 [4815-2018](https://doi.org/10.5194/hess-22-4815-2018)
- 1053 Skofronick-Jackson, G., Petersen, W.A., Berg, W., Kidd, C., Stocker, E.F., Kirschbaum, D.B., Kakar,
1054 R., Braun, S.A., Huffman, G.J., Iguchi, T., Kirstetter, P.E., Kummerow, C., Meneghini, R., Oki,
1055 R., Olson, W.S., Takayabu, Y.N., Furukawa, K., Wilheit, T., 2017. The global precipitation
1056 measurement (GPM) mission for science and Society. *Bull Am Meteorol Soc* 98, 1679–
1057 1695. <https://doi.org/10.1175/BAMS-D-15-00306.1>
- 1058 Song, X.P., Hansen, M.C., Potapov, P., Adusei, B., Pickering, J., Adami, M., Lima, A., Zalles, V.,
1059 Stehman, S. v., di Bella, C.M., Conde, M.C., Copati, E.J., Fernandes, L.B., Hernandez-Serna,
1060 A., Jantz, S.M., Pickens, A.H., Turubanova, S., Tyukavina, A., 2021. Massive soybean
1061 expansion in South America since 2000 and implications for conservation. *Nat Sustain* 4,
1062 784–792. <https://doi.org/10.1038/s41893-021-00729-z>

- 1063 Song, X.P., Hansen, M.C., Stehman, S. v., Potapov, P. v., Tyukavina, A., Vermote, E.F.,
1064 Townshend, J.R., 2018. Global land change from 1982 to 2016. *Nature* 560, 639–643.
1065 <https://doi.org/10.1038/s41586-018-0411-9>
- 1066 Strasser, M.A., 2008. DUNAS FLUVIAIS NO RIO SOLIMÕES-AMAZONAS-DINÂMICA E TRANSPORTE
1067 DE SEDIMENTOS (Tese). Universidade Federal do Rio de Janeiro, Rio de Janeiro.
- 1068 Swanson, A.C., Bohlman, S., 2021. Cumulative Impacts of Land Cover Change and Dams on the
1069 Land–Water Interface of the Tocantins River. *Front Environ Sci* 9.
1070 <https://doi.org/10.3389/fenvs.2021.662904>
- 1071 Syvitski, J.P.M., Kettner, A.J., Overeem, I., Hutton, E.W.H., Hannon, M.T., Brakenridge, G.R., Day,
1072 J., Vörösmarty, C., Saito, Y., Giosan, L., Nicholls, R.J., 2009. Sinking deltas due to human
1073 activities. *Nat Geosci* 2, 681–686. <https://doi.org/10.1038/ngeo629>
- 1074 Syvitski, J.P.M., Vörösmarty, C.J., Kettner, A.J., Green, P., 2005. Impact of Humans on the Flux of
1075 Terrestrial Sediment to the Global Coastal Ocean. *Science* (1979) 308, 376–380.
- 1076 SZUPIANY, R., TRENTO, A., ALVAREZ, A., 2005. Transporte de Sedimentos de Fondo en el Rio
1077 Salado (Santa Fe, Argentina). *Revista Brasileira de Recursos Hídricos* 10, 79–88.
1078 <https://doi.org/10.21168/rbrh.v10n1.p79-88>
- 1079 Thorp, J.H., Thoms, M.C., Delong, M.D., 2006. The riverine ecosystem synthesis: Biocomplexity
1080 in river networks across space and time. *River Res Appl* 22, 123–147.
1081 <https://doi.org/10.1002/rra.901>
- 1082 Tilmant, A., Arjoon, D., Marques, G.F., 2014. Economic Value of Storage in Multireservoir
1083 Systems. *J Water Resour Plan Manag* 140, 375–383.
1084 [https://doi.org/10.1061/\(asce\)wr.1943-5452.0000335](https://doi.org/10.1061/(asce)wr.1943-5452.0000335)
- 1085 Vörösmarty, C.J., Meybeck, M., Fekete, B., Sharma, K., Green, P., Syvitski, J.P.M., 2003.
1086 Anthropogenic sediment retention: Major global impact from registered river
1087 impoundments. *Glob Planet Change* 39, 169–190. [https://doi.org/10.1016/S0921-8181\(03\)00023-7](https://doi.org/10.1016/S0921-8181(03)00023-7)
1088
- 1089 Webb, J., Mainville, N., Mergler, D., Lucotte, M., Betancourt, O., Davidson, R., Cueva, E.,
1090 Quizhpe, E., 2004. Mercury in Fish-eating Communities of the Andean Amazon, Napo River
1091 Valley, Ecuador. *Ecohealth* 1, SU59–SU71. <https://doi.org/10.1007/s10393-004-0063-0>
- 1092 Wei, X., Sauvage, S., Le, T.P.Q., Ouillon, S., Orange, D., Vinh, V.D., Sanchez-Perez, J.M., 2019. A
1093 modeling approach to diagnose the impacts of global changes on discharge and suspended
1094 sediment concentration within the Red River Basin. *Water* (Switzerland) 11.
1095 <https://doi.org/10.3390/w11050958>
- 1096 Wiegand, M.C., 2009. Proposta metodológica para estimativa da produção de sedimentos em
1097 grandes bacias hidrográficas: estudo de caso Alto Jaguaribe, CE (Dissertação). Universidade
1098 Federal do Ceará, Fortaleza.

- 1099 Williams, J.R., 1975. Sediment-yield prediction with Universal Equation using runoff energy
1100 factor. *Present and Prospective Technology for Predicting Sediment Yield and Sources ARS-*
1101 *S-40*, 244–252.
- 1102 Wisser, D., Fekete, B.M., Vörösmarty, C.J., Schumann, A.H., 2010. Reconstructing 20th century
1103 global hydrography: A contribution to the Global Terrestrial Network- Hydrology (GTN-H).
1104 *Hydrol Earth Syst Sci* 14, 1–24. <https://doi.org/10.5194/hess-14-1-2010>
- 1105 WU, W., 2008. *Computational River Dynamics*. Taylor & Francis, London.
- 1106 Wu, W., Wang, S.S.Y., 2006. Formulas for Sediment Porosity and Settling Velocity. *Journal of*
1107 *Hydraulic Engineering* 132, 858–862. [https://doi.org/https://doi.org/10.1061/\(ASCE\)0733-](https://doi.org/https://doi.org/10.1061/(ASCE)0733-9429(2006)132:8(858))
1108 [9429\(2006\)132:8\(858\)](https://doi.org/https://doi.org/10.1061/(ASCE)0733-9429(2006)132:8(858))
- 1109 Yamazaki, D., de Almeida, G.A.M., Bates, P.D., 2013. Improving computational efficiency in
1110 global river models by implementing the local inertial flow equation and a vector-based
1111 river network map. *Water Resources Research* 49, 7221–7235.
- 1112 Yigzaw, W., Li, H.-Y., Demissie, Y., Hejazi, M.I., Leung, L.R., Voisin, N., Payn, R., 2018. A New
1113 Global Storage-Area-Depth Dataset for Modeling Reservoirs in Land Surface and Earth
1114 System Models. *Water Resources Research TECHNICAL* 54, 10,372–10,386.
- 1115 Yokoo, E.M., Valente, J.G., Grattan, L., Schmidt, S.L., Platt, I., Silbergeld, E.K., 2003. Low level
1116 methylmercury exposure affects neuropsychological function in adults. *Environ Health* 8.
1117 <https://doi.org/https://doi.org/10.1186/1476-069X-2-8>
- 1118 Zalles, V., Hansen, M.C., Potapov, P. v, Parker, D., Stehman, S. v, Pickens, A.H., Parente, L.L.,
1119 Ferreira, L.G., Song, X.-P., Hernandez-Serna, A., Kommareddy, I., 2021. Rapid expansion of
1120 human impact on natural land in South America since 1985. *Sci. Adv* 7. [https://doi.org/DOI:](https://doi.org/DOI:10.1126/sciadv.abg1620)
1121 [10.1126/sciadv.abg1620](https://doi.org/DOI:10.1126/sciadv.abg1620)
- 1122 Zarfl, C., Lumsdon, A.E., Berlekamp, J., Tydecks, L., Tockner, K., 2015. A global boom in
1123 hydropower dam construction. *Aquat Sci* 77, 161–170. [https://doi.org/10.1007/s00027-](https://doi.org/10.1007/s00027-014-0377-0)
1124 [014-0377-0](https://doi.org/10.1007/s00027-014-0377-0)
- 1125